

## RECOVERY-BASED A POSTERIORI ERROR ESTIMATION FOR ELLIPTIC INTERFACE PROBLEMS BASED ON PARTIALLY PENALIZED IMMERSED FINITE ELEMENT METHODS

YANPING CHEN, ZHIROU DENG, AND YUNQING HUANG

**Abstract.** This paper develops a recovery-based a posteriori error estimation for elliptic interface problems based on partially penalized immersed finite element (PPIFE) methods. Due to the low regularity of solution at the interface, standard gradient recovery methods cannot obtain superconvergent results. To overcome this drawback a new gradient recovery method is proposed that applies superconvergent cluster recovery (SCR) operator on each subdomain and weighted average (WA) operator at recovering points on the approximated interface. We prove that the recovered gradient superconverges to the exact gradient at the rate of  $O(h^{1.5})$ . Consequently, the proposed method gives an asymptotically exact a posteriori error estimator for the PPIFE methods and the adaptive algorithm. Numerical examples show that the error estimator and the corresponding adaptive algorithm are both reliable and efficient.

**Key words.** Interface problems, a posteriori error estimation, immersed finite element methods, gradient recovery, adaptive algorithm.

### 1. Introduction

Interface problems arise in many applications of fluid mechanics and material science, where its governing partial differential equations (PDEs) have discontinuous coefficients. Solving interface problems accurately and efficiently is a challenge because these coefficients across the interface lead to low global regularity of the solution. Finite element (FE) methods for interface problems have been widely studied, which can be roughly divided into two categories: interface-fitted FE methods [1–4] and interface-unfitted FE methods [5–7]. The interface-fitted FE methods require the partition to be aligned with the interface. It is well known that these methods have the optimal convergence rate in both  $L^2$  and energy norms [8, 9] when the exact solution has sufficient regularity. However, it is usually difficult and time-consuming to generate the required body-fitted meshes, especially when the interface geometry is complex. There are increasing interests in developing interface-unfitted FE methods using interface-unfitted meshes. The immersed finite element (IFE) methods proposed by Li et al. [10, 11] are based on finite element discretizations on interface-unfitted meshes. The main idea of IFE methods is to construct basis functions satisfying the jump conditions on the interface elements to obtain sharp solutions around the interface. In [12], Li et al. proved that the IFE space has the optimal approximation capability. However, Chou et al. showed in [13] that the non-conforming IFE methods do not have fully second order accuracy. It is second order in the  $L^2$  norm, but only first order convergence in the  $L^\infty$  norm due to the consistent error resulted from the discontinuities of test functions. Some improved IFE methods have been developed to eliminate the consistent error,

for instance, symmetric and consistent immersed finite element (SCIFE) methods [14], Petrov-Galerkin immersed finite element (PGIFE) methods [15] and partially penalized immersed finite element (PPIFE) methods [6] and so on.

Compared with the standard IFE methods, PPIFE methods introduce extra stabilization terms only at the interface edges for penalizing the inter-element discontinuity. The optimal convergence rate is theoretically proved for the PPIFE methods in the energy norm and  $L^2$  norm [6, 16]. Moreover, the PPIFE methods were extended to the semi-linear elliptic interface problems [17], the second-order elliptic interface problems with non-homogeneous jump conditions in [18], and other types of interface problems in [19, 20].

Error analysis is a classic topic in FE methods, and it is typically categorized into a priori and a posteriori error estimates. The a priori error estimates of IFE methods have been well developed in the past decade, but the a posteriori error estimates of IFE methods are still in the initial stage. Cao et al. [21] introduced a new approach for constructing IFE basis functions based on the theory of orthogonal polynomials. They proved that IFE methods for one dimensional general elliptic interface problems have nodal superconvergence at the roots of generalized orthogonal polynomials. For two dimensional cases, Guo et al. [22] designed an improved polynomial preserving recovery (IPPR) method for SCIFE and PGIFE methods, and verified its superconvergence by numerical examples. In [23], they also showed the supercloseness results for PPIFE methods and proved that the recovered gradient using the IPPR operator is superconvergent to the exact gradient. He et al. [24] proposed and analyzed the residual-based a posteriori error estimation of the PPIFE methods for solving elliptic interface problems. The a posteriori error estimate is proved to be reliable and efficient.

The purpose of this paper is to develop and analyze a novel recovery-based a posteriori error estimation of the PPIFE methods for elliptic interface problems. Standard gradient recovery methods, including superconvergent patch recovery (SPR) [25, 26], polynomial preserving recovery (PPR) [27–29] and superconvergent cluster recovery (SCR) [30], cannot obtain the superconvergent recovered gradient due to the low regularity of numerical solution at the interface. A recovery-based a posteriori error estimator based on these methods will result in over-refinement as studied in [31]. Therefore, these methods cannot be directly applied to the interface problems. Note that the SCR method obtains the recovered gradient at recovering points by taking derivatives of a linear polynomial, in which the linear polynomial is acquired by least-square fitting the solution values in a cluster of sampling points. This recovery procedure is simpler and effective, and maintains the superconvergence properties of SPR and PPR methods [30]. Hence, our gradient recovery method is based on the SCR method.

In this paper, we propose a new gradient recovery operator for PPIFE methods, and prove that the operator is linear, bounded, and consistent. The establishment of the operator relies on three observations: (i) IFE solution is piecewise smooth on each subdomain, although it has low global regularity; (ii) the solution is discontinuous at the interface, even if the exact solution is continuous; (iii) the SCR operator is local. Accordingly, the gradient recovery operator is constructed by two steps: enriching and smoothing. We first design an enriching operator to make the discontinuous FE solution continuous on a local body-fitted mesh generated by adding extra nodes [10], and then apply the SCR operator to the enriched FE

solution on each subdomain. One also notices that the SCR operator cannot accurately obtain the steep gradient at the interface. To overcome the difficulty, we change the gradient recovery approach of the SCR operator at recovering points on the approximation interface. For simplicity, we draw on the idea of the weighted average (WA) gradient recovery method. More specifically, for the recovering point away from the interface, we use the standard SCR operator. For the recovering point close to the interface, we design a gradient recovery operator to obtain the derivative of a linear polynomial, where the polynomial is acquired by least-square fitting the solution values of the sampling points only in each subdomain. For the recovering point on the approximated interface, we use the WA gradient recovery operator.

Furthermore, we prove that the recovered gradient using our operator superconverges to the exact gradient, and the corresponding a posteriori error estimator is asymptotically exact. Finally, we combine the PPIFE methods with the adaptive technique to solve the elliptic interface problems, and apply the derived a posteriori error estimation to control the adaptive mesh refinement. Numerical experiments show that a posteriori error estimator and adaptive algorithm for the proposed gradient recovery method are robust and effective.

The rest of the paper is organized as follows. In Section 2, we introduce some notations and PPIFE methods. In Section 3, we review superconvergent cluster recovery and enriching operator. Based on this, we design a new gradient recovery method of PPIFE methods to elliptic interface problems, and give a recovery-based a posteriori error estimator. Section 4 is devoted to the analysis of a posteriori error estimation. Finally, in Section 5, several numerical examples are given to verify the performance of our recovery-based a posteriori error estimator.

## 2. Partially Penalized IFE for Elliptic Interface Problems

Let  $\Omega$  be a bounded and convex domain with Lipschitz continuous boundary  $\partial\Omega$  in  $\mathbb{R}^2$ , which is separated by a  $C^2$ -curve interface  $\Gamma$  into two disjoint subdomains  $\Omega^+$  and  $\Omega^-$  satisfying  $\bar{\Omega} = \bar{\Omega}^+ \cup \bar{\Omega}^- \cup \Gamma$ . We consider the following elliptic interface problem with the homogeneous Dirichlet boundary condition:

$$(1) \quad \begin{cases} -\nabla \cdot (\beta(z)\nabla u) = f, & z \in \Omega \setminus \Gamma, \\ u = 0, & z \in \partial\Omega, \end{cases}$$

and the exact solution  $u$  is assumed to satisfy the interface jump conditions:

$$(2) \quad \begin{cases} [u]|_{\Gamma} = u^+ - u^- = 0, \\ \left[ \beta \frac{\partial u}{\partial \mathbf{n}} \right]_{\Gamma} = \beta^+ \frac{\partial u^+}{\partial \mathbf{n}} - \beta^- \frac{\partial u^-}{\partial \mathbf{n}} = 0, \end{cases}$$

where  $u^{\pm} = u|_{\Omega^{\pm}}$  and  $\mathbf{n}$  is the unit outward normal to the boundary  $\partial\Omega$ . And the diffusion coefficient  $\beta(z)$  is a positive piecewise constant function, i.e.

$$(3) \quad \beta(z) = \begin{cases} \beta^+, & \text{for } z \in \Omega^+, \\ \beta^-, & \text{for } z \in \Omega^-. \end{cases}$$

We use the standard notations for the Sobolev spaces. Let

$$H_0^1(\Omega) = \{u \in H^1(\Omega) : u = 0 \text{ on } \partial\Omega\}.$$

Then the variational problem for the elliptic interface problem (1)-(2) is to find  $u \in H_0^1(\Omega)$  such that

$$(4) \quad a_h(u, v) \triangleq (\beta \nabla u, \nabla v) = (f, v), \quad \forall v \in H_0^1(\Omega),$$

where  $(\cdot, \cdot)$  is the  $L^2$  inner product on the domain  $\Omega$ .

**2.1. Preliminaries.** In this paper, we let  $C$  be a generic positive constant which may take different values on different cases, and  $\mathbb{P}_m(\cdot)$  be the polynomial space of degree less than or equal to  $m$ .  $W^{k,p}(\Omega)$  denotes the Sobolev space on  $\Omega$  with norm  $\|\cdot\|_{k,p,\Omega}$  and seminorm  $|\cdot|_{k,p,\Omega}$ . When  $p = 2$ , let  $H^k(\Omega) = W^{k,2}(\Omega)$ ,  $\|\cdot\|_{k,\Omega} = \|\cdot\|_{k,2,\Omega}$ ,  $|\cdot|_{k,\Omega} = |\cdot|_{k,2,\Omega}$ . For theoretical analysis, we define the piecewise Sobolev space

$$W^{k,p}(\Omega^+ \cup \Omega^-) = \{v \in W^{1,p}(\Omega) : v|_{\Omega^s} \in W^{k,p}(\Omega^s), s = +, -\},$$

equipped with the norm

$$\|v\|_{k,p,\Omega^+ \cup \Omega^-} = \left( \|v\|_{k,p,\Omega^+}^p + \|v\|_{k,p,\Omega^-}^p \right)^{\frac{1}{p}}, \quad \forall v \in W^{k,p}(\Omega^+ \cup \Omega^-),$$

and seminorm

$$|v|_{k,p,\Omega^+ \cup \Omega^-} = \left( |v|_{k,p,\Omega^+}^p + |v|_{k,p,\Omega^-}^p \right)^{\frac{1}{p}}, \quad \forall v \in W^{k,p}(\Omega^+ \cup \Omega^-).$$

Similarly, when  $p = 2$ , we define  $H^k(\Omega^+ \cup \Omega^-) = W^{k,2}(\Omega^+ \cup \Omega^-)$ , and the subscript  $p$  of its associate norm and seminorm is omitted.

Assume that the domain  $\Omega$  is partitioned by a Cartesian triangulation  $\mathcal{T}_h = \{T\}$ ,  $h = \max_{T \in \mathcal{T}_h} \text{diam}(T)$ . Here the edges of element  $T \in \mathcal{T}_h$  are not needed to align the interface  $\Gamma$ . For triangulation  $\mathcal{T}_h$ , denote the set of all interior edges by  $\tilde{\mathcal{E}}_h = \tilde{\mathcal{E}}_h^i \cup \tilde{\mathcal{E}}_h^n$ , where  $\tilde{\mathcal{E}}_h^i = \{e \in \tilde{\mathcal{E}}_h : e \cap \Gamma \neq \emptyset\}$  and  $\tilde{\mathcal{E}}_h^n = \tilde{\mathcal{E}}_h \setminus \tilde{\mathcal{E}}_h^i$ . Moreover, denote by  $\mathcal{N}_h$  the set of vertices of all elements in the triangulation  $\mathcal{T}_h$ .

For every interior edge  $e \in \tilde{\mathcal{E}}_h$ , there exist two neighboring elements  $T_{e,1}$  and  $T_{e,2}$  sharing the common edge  $e$ . We let  $\mathbf{n}_e$  be the unit normal vector of  $e$  pointing from  $T_{e,1}$  to  $T_{e,2}$ . For  $v \in T_{e,1} \cup T_{e,2}$ , define its jump and average on the edge  $e$  by

$$[v]_e = v|_{T_{e,1}} - v|_{T_{e,2}}, \quad \{v\}_e = \frac{1}{2}(v|_{T_{e,1}} + v|_{T_{e,2}}).$$

Usually, the subscript  $e$  in  $[\cdot]$  and  $\{\cdot\}$  can be omitted if there is no confusion.

For simplicity, we assume that the interface  $\Gamma$  does not intersect the boundary and cuts two different edges of the element at most once, which holds when  $h$  is small enough. If interface  $\Gamma$  passes through the interior of an element  $T$ , we call it an interface element and denote by  $\mathcal{T}_h^i$  the set of all interface elements; otherwise, an element is called the non-interface element, and its set is denoted by  $\mathcal{T}_h^n$ . In addition, we denote the approximated interface by  $\Gamma_h$  which is composed of all line segments connecting the intersections of the interface and elements.

**2.2. Partially Penalized Immersed Finite Element Methods.** The key idea of the immersed finite element methods is to construct piecewise linear basis functions on the interface elements to satisfy (completely or approximately) the interface jump conditions (2). Then, we introduce the IFE space  $V_h$ .

For any element  $T \in \mathcal{T}_h^n$ , we use standard linear nodal basis functions. However, these basis functions cannot be used for interface elements, because it only satisfies  $[u]_\Gamma = 0$ , not the jump conditions  $[\beta \frac{\partial u}{\partial \mathbf{n}}]_\Gamma = 0$ . Therefore, the basis functions on the interface elements need to be modified to satisfy the interface jump condition.

For any element  $T \in \mathcal{T}_h^i$ , we introduce the construction of the basis functions on the interface elements by the typical interface element  $T = \triangle ABC$  as shown in Figure 1.

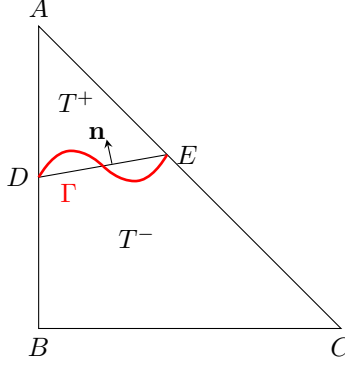


FIGURE 1. A typical interface element  $T$ .

Let  $D$  and  $E$  be the intersections of the interface  $\Gamma$  and the edges of the element. Then the element  $T$  is divided into two parts  $T^+ = T \cap \Omega^+$  and  $T^- = T \cap \Omega^-$  by using the line segment  $\overline{DE}$  as the approximation of the interface  $\Gamma$  in the element  $T$ . We construct a piecewise linear function on the interface element  $T$  as follows:

$$(5) \quad \phi(z) = \begin{cases} \phi^+(z) = a^+ + b^+x + c^+y, & z = (x, y) \in T^+, \\ \phi^-(z) = a^- + b^-x + c^-y, & z = (x, y) \in T^-, \end{cases}$$

where the coefficients satisfy the interface jump conditions:

$$(6) \quad \phi^+(D) = \phi^-(D), \quad \phi^+(E) = \phi^-(E), \quad \beta^+ \frac{\partial \phi^+}{\partial \mathbf{n}} = \beta^- \frac{\partial \phi^-}{\partial \mathbf{n}},$$

and the Lagrange conditions:

$$(7) \quad \phi(A) = V_1, \quad \phi(B) = V_2, \quad \phi(C) = V_3,$$

with  $\mathbf{n}$  being the unit normal of  $\overline{DE}$  and  $V_i, i = 1, 2, 3$  being the nodal variables.

We now introduce the following local finite element space on each element  $T \in \mathcal{T}_h$ :

$$V_h(T) = \begin{cases} \{v(z) : v(z) \text{ is linear on } T\}, & \text{if } T \in \mathcal{T}_h^n, \\ \{v(z) : v(z) \text{ is defined by (5) - (7)}\}, & \text{if } T \in \mathcal{T}_h^i. \end{cases}$$

Then, the IFE space  $V_h$  over the whole region  $\Omega$  is defined to contain all functions such that

- (I)  $v|_T \in V_h(T)$  for all  $T \in \mathcal{T}_h$ ;
- (II)  $v$  is continuous at every vertex  $X \in \mathcal{N}_h$ .

The PPIFE methods for the interface problem (1)-(2): find  $u_h \in V_{h,0} = \{u \in V_h : u|_{\partial\Omega} = 0\}$  such that

$$(8) \quad a_h(u_h, v_h) = (f, v_h), \quad \forall v_h \in V_{h,0},$$

where the bilinear form  $a_h(\cdot, \cdot) : V_{h,0} \times V_{h,0} \rightarrow \mathbb{R}$  is defined by

$$\begin{aligned}
 (9) \quad a_h(v_h, w_h) &= \sum_{T \in \mathcal{T}_h} \int_T \beta \nabla v_h \cdot \nabla w_h \, dX - \sum_{e \in \tilde{\mathcal{E}}_h^i} \int_e \{\beta \nabla v_h \cdot \mathbf{n}_e\} [w_h] \, ds \\
 &+ \epsilon \sum_{e \in \tilde{\mathcal{E}}_h^i} \int_e \{\beta \nabla w_h \cdot \mathbf{n}_e\} [v_h] \, ds \\
 &+ \sum_{e \in \tilde{\mathcal{E}}_h^i} \int_e \frac{\sigma_e^0}{|e|^\gamma} [v_h] [w_h] \, ds, \quad \forall v_h, w_h \in V_{h,0},
 \end{aligned}$$

where  $|e|$  is the length of  $e$ , the parameter  $\sigma_e^0 \geq 0, \gamma > 0$  and  $\epsilon$  is arbitrary.  $\epsilon$  usually takes the value -1, 0 or 1. Obviously, the bilinear form  $a_h(\cdot, \cdot)$  is symmetric only when  $\epsilon = -1$ , and others are non-symmetric.

We introduce the energy norm as follow:

$$(10) \quad \|v_h\|_h = \left( \sum_{T \in \mathcal{T}_h} \int_T \beta \nabla v_h \cdot \nabla v_h \, dx + \sum_{e \in \tilde{\mathcal{E}}_h^i} \int_e \frac{\sigma_e^0}{|e|^\gamma} [v_h] [v_h] \, ds \right)^{\frac{1}{2}}.$$

In [6], the coercivity of the bilinear form  $a_h(\cdot, \cdot)$  has been proved, namely, there exists a constant  $C > 0$  such that

$$(11) \quad C \|v_h\|_h^2 \leq a_h(v_h, v_h), \quad \forall v_h \in V_{h,0},$$

is true for  $\epsilon = 1$  unconditionally and is true for  $\epsilon = -1$  or  $\epsilon = 0$  under the condition that the parameter  $\sigma_e^0$  in  $a_h(\cdot, \cdot)$  is large enough.

Based on the above coercivity, the following optimal convergence result is proved in [16].

**Lemma 2.1.** *Let  $u \in H^2(\Omega^+ \cup \Omega^-)$  be the exact solution of the interface problem (1)-(2) and  $u_h$  be the PPIFE solution of (8) generated with  $\gamma = 1$  on a Cartesian mesh  $\mathcal{T}_h$ . Then there exists a constant  $C$ , such that*

$$(12) \quad \|u - u_h\|_h \leq Ch \|u\|_{2, \Omega^+ \cup \Omega^-}.$$

**Remark 2.1.** *As stated in the remark of [6], if  $u \in W^{2, \infty}(\Omega^+ \cup \Omega^-)$  is the exact solution of the interface problem (1)-(2),  $u_h$  is the PPIFE solution of (8) generated with  $\gamma = 1$  on a Cartesian mesh  $\mathcal{T}_h$ . Then the error estimation is*

$$(13) \quad \|u - u_h\|_h \leq C \left( h \|u\|_{2, \Omega^+ \cup \Omega^-} + h^{\frac{3}{2}} \|u\|_{2, \infty, \Omega^+ \cup \Omega^-} \right).$$

### 3. Gradient Recovery for PPIFE Methods

In this section, we first summarize the superconvergent cluster recovery (SCR) method in [30]. Then, we define an enriching operator that makes discontinuous FE solution continuous, and finally propose an improved SCR gradient recovery method for the elliptic interface problems.

**3.1. Superconvergent Cluster Recovery.** The key idea of the SCR method is that it fits a linear polynomial function to the FE solution values at a group of symmetrical sampling points, from which the recovered gradient can be obtained at the recovering point.

Let  $\widehat{\mathcal{T}}_h$  be a triangulation of  $\Omega \subset \mathbb{R}^2$  and  $\widehat{\mathcal{N}}_h$  be the set of vertices of all elements. Consider the  $C^0$  linear FE space  $\widehat{X}_h$  associated with  $\widehat{\mathcal{T}}_h$ . The standard Lagrange basis of  $\widehat{X}_h$  is denoted by  $\{\phi_z : z \in \widehat{\mathcal{N}}_h\}$ , such that

$$\phi_z(z') = \delta_{zz'}, \quad \forall z, z' \in \widehat{\mathcal{N}}_h,$$

where  $\delta_{zz'}$  is Kronecker delta function. Next, we describe SCR operator  $G_h : \widehat{X}_h \rightarrow \widehat{X}_h \times \widehat{X}_h$  and its properties.

For any  $v_h \in \widehat{X}_h$ , the recovered gradient  $G_h v$  on the domain  $\Omega$  is obtained by the interpolation. If  $\{(G_h v)(z) : z \in \widehat{\mathcal{N}}_h\}$  is defined, then

$$(14) \quad G_h v = \sum_{z \in \widehat{\mathcal{N}}_h} (G_h v)(z) \phi_z, \quad z \in \widehat{\mathcal{N}}_h.$$

For any interior vertex  $z = z_0 = (x_0, y_0) \in \widehat{\mathcal{N}}_h$ , we select some points  $z_i = (x_i, y_i)$ ,  $1 \leq i \leq n$ ,  $n \geq 4$  as sampling points so that they are as symmetrical as possible around vertex  $z$ , see Figure 2 (a). In general, selecting the mesh nodes behaved well. Let  $\mathcal{K}_z$  be a convex polygon of the sampling points. We obtain the linear polynomial  $p_z \in \mathbb{P}_1(\mathcal{K}_z)$  by least-square fitting the function value  $v(z_i)$  at those sampling points, i.e.

$$(15) \quad p_z = \arg \min_{p_1 \in \mathbb{P}_1(\mathcal{K}_z)} \sum_{i=0}^n (p_1(z_i) - v(z_i))^2, \quad v \in \widehat{X}_h.$$

Therefore, the recovered gradient at the interior vertex  $z$  is defined as

$$(16) \quad (G_h v)(z) = \nabla p_z(z).$$

For any  $z \in \partial\Omega$ , similar to SPR method, the recovered gradient is obtained from the interior vertices connected by the boundary point. Specifically, we define  $(G_h v)(z)$  based on the location of  $z$ :

(I) If  $z \in \partial\Omega$  and there is no interior vertices directly adjacent to it, see Figure 2 (b), the recovered gradient at  $z$  is defined to be

$$(17) \quad (G_h v)(z) = \nabla v_h(z).$$

(II) If  $z \in \partial\Omega$  and there are some interior vertices  $z_1, z_2, \dots, z_{N_z}$  directly adjacent to it, see Figure 2 (c), we first find the linear polynomial  $p_{z_i}(z)$ ,  $i = 1, 2, \dots, N_z$ , and then define the recovered gradient at  $z$  by

$$(18) \quad (G_h v)(z) = \frac{1}{N_z} \sum_{i=1}^{N_z} \nabla p_{z_i}(z).$$

In the following, we summarize the properties of the SCR operator, which has been proved in [30].

**Lemma 3.1.** *For the SCR operator  $G_h$ , we have*

(I) **Linearity.**  $G_h$  is a linear operator.

(II) **Boundedness.** For any element  $T \in \widehat{\mathcal{T}}_h$ , there exists a constant  $C$  independent of the mesh size  $h$  such that

$$(19) \quad \|G_h v\|_{0,T} \leq C|v|_{1,\widehat{\omega}_T}, \quad \forall v \in \widehat{X}_h,$$

where  $\widehat{\omega}_T = \cup_{i=1}^3 T_i$  with  $T_i$  is the elements which include the sampling points of the  $i$ th vertex of  $T$ .

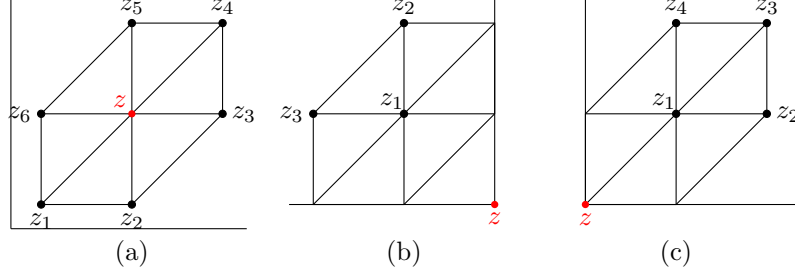


FIGURE 2. Interior vertices connected by the recovering point  $z$ . (a)  $z$  is the interior vertex; (b)  $z$  is the boundary vertex and not adjacent to the interior points; (c)  $z$  is the boundary vertex and adjacent to the interior points.

(III) **Superconvergence.** Let  $z_i = (x_i, y_i), 1 \leq i \leq n, n \geq 4$  be the equally distributed sampling points on the circle, and the recovering point  $z = z_0 = (x_0, y_0)$  be the circle center. Then we have

$$(20) \quad |\nabla v(z) - (G_h v)(z)| \leq Ch^{1+\rho}, \quad \forall v \in W^{3,\infty}(\omega_z),$$

where  $\rho \in (0, 1]$  and  $\omega_z$  is a union of elements covering the sampling points required for the recovery of  $(G_h v)(z)$ .

**Remark 3.1.** The selection of sampling points influences the SCR method, and the symmetry of sampling points about recovering points is the key to the superconvergence of the SCR method. See [30] for detailed analysis.

Based on the above properties of SCR method, we can deduce the following approximation property.

**Lemma 3.2.** Let  $G_h : \widehat{X}_h \rightarrow \widehat{X}_h \times \widehat{X}_h$  be the SCR gradient recovery operator. There exists a constant  $C$  independent of the mesh size  $h$ , such that

$$(21) \quad \|\nabla v - G_h v_I\|_{0,\Omega} \leq Ch^2(|v|_{3,\Omega} + |v|_{2,\infty,\Omega}), \quad \forall v \in H^3(\Omega) \cap W^{2,\infty}(\Omega),$$

where  $v_I$  is a linear interpolation of  $v$  in  $\widehat{X}_h$ .

*Proof.* Form the boundedness of SCR operator (19) and the triangle inequality, we have

$$(22) \quad \|\nabla v - G_h v_I\|_{0,\Omega} \leq \|\nabla v - I_h(\nabla v)\|_{0,\Omega} + \|I_h(\nabla v) - G_h v_I\|_{0,\Omega} + \|G_h v - G_h v_I\|_{0,\Omega},$$

where  $I_h(\nabla v)$  is a piecewise continuous linear vector function on  $\widehat{\mathcal{T}}_h$ , satisfying

$$(23) \quad I_h(\nabla v)(z) = \nabla v(z), \quad \forall z \in \widehat{\mathcal{N}}_h.$$

Then, by the interpolation error estimate

$$(24) \quad \|\nabla v - I_h(\nabla v)\|_{0,\Omega} \leq Ch^2|v|_{3,\Omega}.$$

From the superconvergence of SCR operator, we know that

$$(25) \quad |\nabla v(z) - (G_h v)(z)| \leq Ch^{1+\rho}|v|_{3,\omega_z}, \quad \forall z \in \widehat{\mathcal{N}}_h.$$

Then, applying the fact that  $I_h(\nabla v)$  and  $G_h v$  are piecewise continuous linear vector function gives

$$\begin{aligned} \|I_h(\nabla v) - G_h v\|_{0,T} &\leq C\sqrt{|T|} \|I_h(\nabla v) - G_h v\|_{0,\infty,T} \\ &\leq Ch \max_{z \in T} |I_h(\nabla v)(z) - (G_h v)(z)| \\ &\leq Ch \max_{z \in T} |\nabla v(z) - (G_h v)(z)| \\ &\leq Ch^{2+\rho} |v|_{3,\omega_z}, \end{aligned}$$

where  $|T|$  is the area of  $T$ . Summarizing the above inequalities indicates

$$\|I_h(\nabla v) - G_h v\|_{0,\Omega}^2 \leq \sum_{T \in \hat{\mathcal{T}}_h} \|I_h(\nabla v) - G_h v\|_{0,T}^2 \leq Ch^{2(2+\rho)} |v|_{3,\Omega}^2.$$

Therefore,

$$(26) \quad \|I_h(\nabla v) - G_h v\|_{0,\Omega} \leq Ch^{2+\rho} |v|_{3,\Omega}.$$

For any  $z = z_0 = (x_0, y_0) \in \hat{\mathcal{N}}_h$ , let  $\{z_i = (x_i, y_i), 1 \leq i \leq n, n \geq 4\}$  be the sampling points,  $l_z = \max\{|x_i - x_0|, |y_i - y_0| : 1 \leq i \leq n, n \geq 4\}$ ,  $e_i$  be the line segment connecting the sampling point  $z_i$  and the recovering point  $z$ , and  $h_i$  be the length of  $e_i$ . In [30], it is proved that the SCR recovered gradient can be expressed as a linear combination of the directional derivatives along  $e_i$ :

$$(27) \quad (G_h v)(z) - (G_h v_I)(z) = \left( \begin{array}{c} \frac{-1}{|B|} \sum_{i=1}^n \frac{h_i}{l_z} c_i^1 \frac{v(z_i) - v_I(z_i)}{h_i} \\ \frac{-1}{|B|} \sum_{i=1}^n \frac{h_i}{l_z} c_i^2 \frac{v(z_i) - v_I(z_i)}{h_i} \end{array} \right).$$

Denote by  $T_i$  the element containing  $z_i$ , and the three vertices of  $T_i$  are  $z_j, 1 \leq j \leq 3$ . Let  $l_j = \|z_i - z_j\|$  be the length of line segment  $\overline{z_i z_j}$  and  $\lambda_j$  be the area coordinate. Form the Taylor expansion, one obtains

$$(28) \quad v_I(z_i) - v(z_i) = \frac{1}{2} \sum_{i=1}^3 D^2 v(\xi) l_j^2 \lambda_j(z_i).$$

Substituting (28) into (27), we get

$$|(G_h v)(z) - (G_h v_I)(z)| \leq Ch |v|_{2,\infty,\Omega}.$$

Consequently,

$$(29) \quad \begin{aligned} \|G_h v - G_h v_I\|_{0,\Omega} &\leq Ch \|G_h v - G_h v_I\|_{0,\infty,\Omega} \\ &= Ch \max_{z \in \Omega} |(G_h v)(z) - (G_h v_I)(z)| \\ &\leq Ch^2 |v|_{2,\infty,\Omega}. \end{aligned}$$

Combining (22), (24), (26) and (29) yields

$$(30) \quad \begin{aligned} \|\nabla v - G_h v_I\|_{0,\Omega} &\leq C(h^2 |v|_{3,\Omega} + h^{2+\rho} |v|_{3,\Omega} + h^2 |v|_{2,\infty,\Omega}) \\ &\leq Ch^2 (|v|_{3,\Omega} + |v|_{2,\infty,\Omega}). \end{aligned}$$

This completes the proof of the lemma.  $\square$

**3.2. Immersed Superconvergent Cluster Recovery.** The standard SCR operator cannot be directly applied to elliptic interface problems for the following three reasons. Firstly, the IFE solution is discontinuous at the interface, and superconvergence results are obtained only when the solution is smooth enough. Secondly, the recovered gradient  $G_h v_h$  is a piecewise continuous linear vector function, while the exact gradient is discontinuous at the interface. Finally, the SCR method does not accurately recover the steep gradient at the interface. Note that the IFE solution is piecewise smooth on each subdomain although its global regularity is low, and SCR and WA gradient recovery methods are local. Therefore, we first establish an enriching operator. Then we construct a gradient recovery operator which applies the standard SCR operator on each subdomain to the enriched FE solution and adopts the WA gradient recovery method to recover the gradient of the recovering point on the approximated interface.

**3.2.1. Enriching operator.** The key idea of the enriching operator is to assign values to the nodes of the local body-fitted mesh  $\widehat{\mathcal{T}}_h$  generated based on the mesh  $\mathcal{T}_h$ , so that the FE solution is continuous at the nodes.

To introduce the enriching operator, we first generate mesh  $\widehat{\mathcal{T}}_h$  consisting of the following triangles [10, 22]:

- (I) For any  $T \in \mathcal{T}_h^n$ , it remains unchanged.
- (II) For any  $T \in \mathcal{T}_h^i$ , split it into three sub-triangles. Firstly,  $T$  is divided into a quadrilateral and a triangle by connecting two intersection points. Then, an auxiliary line connecting an intersection point and a vertex of the element  $T$  is selected to separate the quadrilateral into two triangles, and at least one angle of the two triangles is between  $\frac{\pi}{4}$  and  $\frac{3\pi}{4}$ .

**Remark 3.2.** *We point out that the triangulation  $\widehat{\mathcal{T}}_h$  may contain narrow triangles, which causes the standard linear FE method to deteriorate. However, the introduction of the local body-fitted mesh  $\widehat{\mathcal{T}}_h$  is only to enrich the existing IFE solutions, rather than directly solving the interface problems on it.*

Based on the mesh  $\widehat{\mathcal{T}}_h$ , the enriching operator  $E_h : V_h \rightarrow \widehat{X}_h$  is defined [22]

$$(31) \quad (E_h v)(z) = \frac{1}{|\widehat{\omega}_z|} \sum_{\widehat{T} \in \widehat{\omega}_z} v_{\widehat{T}}(z), \quad \forall z \in \widehat{\mathcal{N}}_h,$$

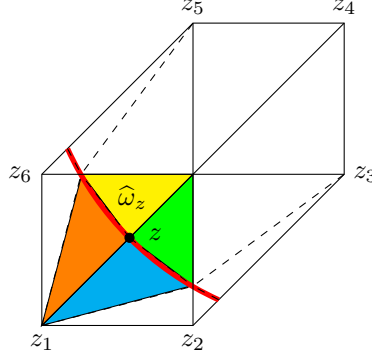
where  $\widehat{\omega}_z$  is the set of all triangles with vertex  $z$  in  $\widehat{\mathcal{T}}_h$  (see Figure 3),  $|\widehat{\omega}_z|$  is the cardinality of  $\widehat{\omega}_z$  and  $v_{\widehat{T}} = v|_{\widehat{T}}$ . After the values  $(E_h v)(z)$  is defined at all vertices, the enriched FE solution  $E_h v$  on  $\Omega$  is obtained by interpolation in  $\widehat{X}_h$ . From the definition of  $\widehat{\mathcal{T}}_h$  and  $\widehat{\mathcal{N}}_h$ , we have  $\mathcal{N}_h \subset \widehat{\mathcal{N}}_h$ . Therefore, it is easy to get  $(E_h v)(z) = v(z)$  for any  $z \in \widehat{\mathcal{N}}_h \cap \mathcal{N}_h$ .

Enriching operator  $E_h$  has the following properties [22].

**Lemma 3.3.** *Let  $E_h$  be the enriching operator defined in (31). There exists a constant  $C$  independent of the mesh size  $h$  and the interface location, such that*

$$(32) \quad \|E_h v\|_{0,\Omega} \leq C \|v\|_{0,\Omega}, \quad \forall v \in V_h,$$

$$(33) \quad |E_h v|_{1,\Omega} \leq C |v|_{1,\Omega}, \quad \forall v \in V_h.$$

FIGURE 3. Example of the  $\hat{\omega}_z$ .

**3.2.2. Immersed Superconvergent Cluster Recovery operator.** Assume  $\Gamma_h$  is the approximated interface introduced in Subsection 2.1, and separates the triangulation  $\hat{\mathcal{T}}_h$  into two disjoint sets:

$$(34) \quad \hat{\mathcal{T}}_h^+ := \{T \in \hat{\mathcal{T}}_h | T \text{ belongs to } \overline{\Omega^+}\},$$

$$(35) \quad \hat{\mathcal{T}}_h^- := \{T \in \hat{\mathcal{T}}_h | T \text{ belongs to } \overline{\Omega^-}\}.$$

Let  $\Omega_h^+ = \cup_{T \in \hat{\mathcal{T}}_h^+} T$  be the approximation of  $\Omega^+$ ,  $\hat{\mathcal{N}}_h^+$  be the set of vertices of all elements in  $\hat{\mathcal{T}}_h^+$ , and  $\hat{X}_h^+$  be the  $C^0$  linear finite element space associated with  $\hat{\mathcal{T}}_h^+$ . Similarly, we can define the  $\Omega_h^- = \cup_{T \in \hat{\mathcal{T}}_h^-} T$ ,  $\hat{\mathcal{N}}_h^-$  and  $\hat{X}_h^-$ .

Denote the SCR operator on  $\hat{X}_h^+$  and  $\hat{X}_h^-$  by  $G_h^+$  and  $G_h^-$ , respectively. For any  $u_h \in V_h$ , we define the global gradient recovery operator  $R_h : V_h \rightarrow (\hat{X}_h^+ \times \hat{X}_h^-) \times (\hat{X}_h^+ \times \hat{X}_h^-)$  as follows:

$$(36) \quad (R_h u_h)(z) = \begin{cases} (G_h^+ E_h u_h)(z), & \text{if } z \in \overline{\Omega_h^+}, \\ (G_h^- E_h u_h)(z), & \text{if } z \in \overline{\Omega_h^-}. \end{cases}$$

Gradient recovery operator  $R_h$  is called immersed superconvergent cluster recovery (ISCR) operator.

We summarize the recovery procedure of ISCR operator in Algorithm 1.

**Remark 3.3.** For the recovering points on the approximation interface, the ISCR method draws on the simple average method in the WA gradient recovery method. We point out that the gradient recovery methods for interface problems can also be obtained by referring to the area average and area harmonic average methods. Next, we introduce these two methods, namely, immersed superconvergent cluster recovery - area average (ISCR-AA) method and immersed superconvergent cluster recovery - area harmonic average (ISCR-AH) method.

If  $z$  is far from and close to the interface in each subdomain, both ISCR-AA and ISCR-AH methods apply the ISCR operator to recover the gradient at  $z$ .

If  $z$  is on approximated interface  $\Gamma_h$ , denote the area of element  $T_i$  by  $|T_i|$ . For  $u_h \in V_h$ , then

**Algorithm 1** The ISCR algorithm

For a given Cartesian mesh  $\mathcal{T}_h$  and an IFE solution  $u_h \in V_h$ , the ISCR method obtains the recovered gradient  $G_h u_h$  by the following four steps.

Setp1: Generate a local body-fitted mesh  $\widehat{\mathcal{T}}_h$  based on  $\mathcal{T}_h$  introduced in Subsection 3.2.1.

Setp2: Enrich the IFE solution  $u_h$  at  $z \in \widehat{\mathcal{N}}_h$ .

$$(37) \quad (E_h u_h)(z) = \frac{1}{|\widehat{\omega}_z|} \sum_{\widehat{T} \in \widehat{\omega}_z} u_h|_{\widehat{T}}(z), \quad \forall z \in \widehat{\mathcal{N}}_h,$$

where  $\widehat{\omega}_z$  is the set of all triangles with vertex  $z$  in  $\widehat{\mathcal{T}}_h$  and  $|\widehat{\omega}_z|$  is the cardinality of  $\widehat{\omega}_z$ .

Setp3: Define the ISCR recovered gradient at  $z \in \widehat{\mathcal{N}}_h$ .

- If  $z = z_0 = (x_0, y_0) \in \widehat{\mathcal{N}}_h^+ \cap \Omega_h^+$  (or  $\widehat{\mathcal{N}}_h^- \cap \Omega_h^-$ ) is the vertex on a non-interface element, we select some points  $z_i = (x_i, y_i), 1 \leq i \leq n, n \geq 4$  as sampling points so that they are as symmetrical as possible around vertex  $z$ , see Figure 4 (a). Let  $\mathcal{K}_z$  be a convex polygon of the sampling points. Find a polynomial  $p_z \in \mathbb{P}_1(\mathcal{K}_z)$  satisfying

$$(38) \quad p_z = \arg \min_{p_1 \in \mathbb{P}_1(\mathcal{K}_z)} \sum_{i=0}^n (p_1(z_i) - (E_h u_h)(z_i))^2,$$

and the recovered gradient at the vertex  $z$  is defined as  $(R_h u_h)(z) = \nabla p_z(z)$ .

- If  $z = z_0 = (x_0, y_0) \in \widehat{\mathcal{N}}_h^+ \cap \Omega_h^+$  (or  $\widehat{\mathcal{N}}_h^- \cap \Omega_h^-$ ) is the vertex on an interface element, we select some points  $z_i = (x_i, y_i), 1 \leq i \leq n, n \geq 4$  only from  $\widehat{\mathcal{N}}_h^+$  (or  $\widehat{\mathcal{N}}_h^-$ ) as sampling points so that they locate around vertex  $z$  as symmetrical as possible, see Figure 4 (b). Similarly, we can obtain the recovered gradient at  $z$ .
- If  $z \in \partial\Omega$  and no interior vertices directly adjacent to it, the recovered gradient at  $z$  is defined to be

$$(39) \quad (R_h u_h)(z) = \nabla(E_h u_h)(z).$$

- If  $z \in \partial\Omega$  and there are some interior vertices  $z_1, z_2, \dots, z_{N_z}$  directly adjacent to it, we first obtain the linear polynomial  $p_{z_i}(z), i = 1, 2, \dots, N_z$ , and then define the recovered gradient at  $z$  by

$$(40) \quad (R_h u_h)(z) = \frac{1}{N_z} \sum_{i=1}^{N_z} \nabla p_{z_i}(z).$$

- If  $z$  is on approximated interface  $\Gamma_h$ , denote  $\omega_z$  to be the patch consisting of elements attached to  $z$ . Let  $T_1, \dots, T_{n_z}, T_{n_z+1}, \dots, T_{m_z} \in \omega_z \cap \widehat{\mathcal{T}}_h$  are elements around  $z$ , where  $T_1, \dots, T_{n_z}$  belonging to  $\Omega_h^+$  and  $T_{n_z+1}, \dots, T_{m_z}$  belonging to  $\Omega_h^-$ . Then we define the recovered gradient at the vertex  $z$  by

$$(41) \quad (R_h u_h)(z) = \frac{1}{n_z} \sum_{i=1}^{n_z} \nabla u_h(z)|_{T_i}, \quad (R_h u_h)(z) = \frac{1}{m_z - n_z} \sum_{i=n_z+1}^{m_z} \nabla u_h(z)|_{T_i}.$$

Setp4: The recovered gradient  $R_h u_h$  on the domain  $\Omega$  is obtained by interpolation

$$(42) \quad R_h u_h = \sum_{z \in \widehat{\mathcal{N}}_h} (R_h u_h)(z) \phi_z.$$

where  $\phi_z$  is the standard Lagrange basis of  $V_h$  at the vertex  $z$ .

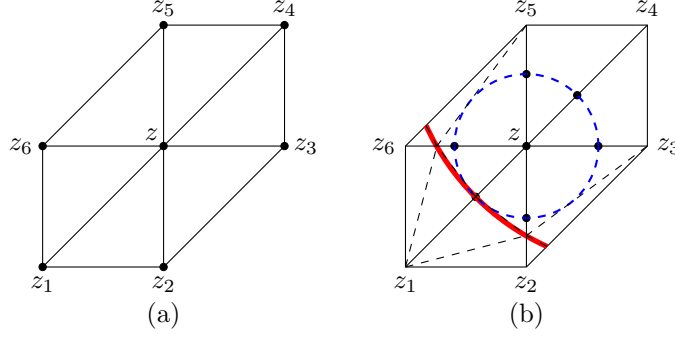


FIGURE 4. Sampling points. (a)  $z$  is the vertex on a non-interface element; (b)  $z$  is the vertex on an interface element.

ISCR-AA method:

$$(43) \quad (S_h u_h)(z) = \sum_{i=1}^{n_z} \frac{|T_i|}{\sum_{j=1}^{n_z} |T_j|} \nabla u_h(z)|_{T_i}, \quad (S_h u_h)(z) = \sum_{i=n_z+1}^{m_z} \frac{|T_i|}{\sum_{j=n_z+1}^{m_z} |T_j|} \nabla u_h(z)|_{T_i}.$$

ISCR-AH method:

$$(44) \quad (H_h u_h)(z) = \sum_{i=1}^{n_z} \frac{1/|T_i|}{\sum_{j=1}^{n_z} 1/|T_j|} \nabla u_h(z)|_{T_i}, \quad (H_h u_h)(z) = \sum_{i=n_z+1}^{m_z} \frac{1/|T_i|}{\sum_{j=n_z+1}^{m_z} 1/|T_j|} \nabla u_h(z)|_{T_i}.$$

It is easy to see that  $R_h$  is a linear operator, and one can prove the boundedness results as follows.

**Lemma 3.4.** *Let  $R_h$  be the ISCR gradient recovery operator. There exists a constant  $C$  independent of the mesh size  $h$  and the interface location, such that*

$$(45) \quad \|R_h u_h\|_{0, \Omega_h^+ \cup \Omega_h^-} \leq C |u_h|_{1, \Omega}, \quad \forall u_h \in V_h.$$

*Proof.* We adopt the boundedness of the standard SCR operator (19) to gain its global boundedness as

$$(46) \quad \|G_h E_h u_h\|_{0, \Omega} \leq C |E_h u_h|_{1, \Omega}, \quad \forall u_h \in V_h.$$

By the definition of ISCR recovery operator, (46) and Lemma 3.3, we have

$$(47) \quad \begin{aligned} \|R_h u_h\|_{0, \Omega_h^+ \cup \Omega_h^-} &\leq \|R_h u_h\|_{0, \Omega_h^+} + \|R_h u_h\|_{0, \Omega_h^-} \\ &= \|G_h^+(E_h u_h)\|_{0, \Omega_h^+} + \|G_h^-(E_h u_h)\|_{0, \Omega_h^-} \\ &\leq C(|E_h u_h|_{1, \Omega_h^+} + |E_h u_h|_{1, \Omega_h^-}) \\ &\leq C |E_h u_h|_{1, \Omega} \\ &\leq C |u_h|_{1, \Omega}. \end{aligned}$$

this completes our proof.  $\square$

Moreover, we have approximation estimate for the ISCR gradient recovery operator  $R_h$ .

**Theorem 3.1.** *Let  $R_h$  be the ISCR gradient recovery operator, and  $u_I$  is linear interpolation of  $u$  in  $\widehat{X}_h$ . Given any  $u \in H^3(\Omega^+ \cup \Omega^-) \cap W^{2,\infty}(\Omega^+ \cup \Omega^-) \cap C^0(\Omega)$ , then the following inequality holds*

$$(48) \quad \|\nabla u - R_h u_I\|_{0,\Omega} \leq Ch^2(\|u\|_{3,\Omega^+ \cup \Omega^-} + \|u\|_{2,\infty,\Omega^+ \cup \Omega^-}),$$

where  $C$  is a constant independent of the mesh size  $h$  and the interface location.

*Proof.* Since  $u \in C^0(\Omega)$ , then  $u_I \in C^0(\Omega)$ . From the definition of enriching operator, we get

$$(49) \quad E_h u_I = u_I.$$

Notice that  $G_h^+$  and  $G_h^-$  are the standard SCR operator, so we get from Lemma 3.2 that

$$(50) \quad \|\nabla u - G_h^+ u_I\|_{0,\Omega_h^+} \leq Ch^2(\|u\|_{3,\Omega^+} + \|u\|_{2,\infty,\Omega^+}),$$

and

$$(51) \quad \|\nabla u - G_h^- u_I\|_{0,\Omega_h^-} \leq Ch^2(\|u\|_{3,\Omega^-} + \|u\|_{2,\infty,\Omega^-}).$$

Hence, we have

$$(52) \quad \begin{aligned} \|\nabla u - R_h u_I\|_{0,\Omega} &\leq \|\nabla u - R_h u_I\|_{0,\Omega_h^+} + \|\nabla u - R_h u_I\|_{0,\Omega_h^-} \\ &= \|\nabla u - G_h^+ E_h u_I\|_{0,\Omega_h^+} + \|\nabla u - G_h^- E_h u_I\|_{0,\Omega_h^-} \\ &\leq \|\nabla u - G_h^+ u_I\|_{0,\Omega_h^+} + \|\nabla u - G_h^- u_I\|_{0,\Omega_h^-} \\ &\leq Ch^2(\|u\|_{3,\Omega^+} + \|u\|_{2,\infty,\Omega^+} + \|u\|_{3,\Omega^-} + \|u\|_{2,\infty,\Omega^-}) \\ &\leq Ch^2(\|u\|_{3,\Omega^+ \cup \Omega^-} + \|u\|_{2,\infty,\Omega^+ \cup \Omega^-}), \end{aligned}$$

which completes the proof.  $\square$

Based on the ISCR operator  $R_h$ , we can define the local error indicator  $\eta_T$  by

$$(53) \quad \eta_T = \begin{cases} \|\beta^{1/2} (R_h u_h - \nabla u_h)\|_{0,T}, & \text{if } T \in \mathcal{T}_h^n, \\ \left( \sum_{\widehat{T} \in \widehat{\mathcal{T}}_h, \widehat{T} \subset T} \|\beta^{1/2} (R_h u_h - \nabla u_h)\|_{0,\widehat{T}}^2 \right)^{\frac{1}{2}}, & \text{if } T \in \mathcal{T}_h^i, \end{cases}$$

and then the global error estimator  $\eta_h$  is defined by

$$(54) \quad \eta_h = \left( \sum_{T \in \mathcal{T}_h} \eta_T^2 \right)^{1/2}.$$

#### 4. A Posteriori Error Estimates based on ISCR operator

In this section, we show that the ISCR gradient recovery method can be applied to PPIFE methods, and prove that the recovered gradient is superconvergent to the exact gradient.

To establish a general framework for proving the superconvergence such as Ainsworth and Oden [32], Chen [33] lists three basic requirements with reference to Yan [34], which are similar to but slightly different from those in [32]. These three requirements are:

(I) **Better approximation.** Let  $v_I \in \widehat{X}_h$  be a linear interpolation of  $v$ . If  $v$  is smooth enough, then

$$\|\nabla v - R_h v_I\|_{0,\Omega} \ll \|\nabla(v - v_I)\|_{0,\Omega}.$$

It is known that  $\|\nabla(v - v_I)\|_{0,\Omega} = O(h)$ , then we have

$$\|\nabla v - R_h v_I\|_{0,\Omega} = O(h^{1+\epsilon}).$$

for some  $\epsilon \in (0, 1]$ .

(II) **Linearity and stability.**  $R_h : V_h \rightarrow (\widehat{X}_h^+ \times \widehat{X}_h^-) \times (\widehat{X}_h^+ \times \widehat{X}_h^-)$  is a linear operator, there exists a constant  $C$  such that

$$(55) \quad \|R_h v\|_{0,T} \leq C|v|_{1,\widehat{\omega}_T}, \quad \forall v \in \widehat{X}_h.$$

(III) **Superclose property.** There exist constant  $C$  and  $\rho \in (0, 1]$  independent of  $h$ , such that

$$(56) \quad \|\nabla(v_I - v_h)\|_{0,\Omega} \leq C(v)h^{1+\rho}.$$

If the FE solution  $v_h$  and the gradient recovery  $R_h$  satisfy the above requirements, we have

$$(57) \quad \|\nabla v - R_h v_h\|_{0,\Omega} \leq Ch^{1+\alpha}, \quad \alpha = \min\{\epsilon, \rho\}.$$

With this superconvergence result, we can easily prove that the corresponding recovery-based a posteriori error estimator is asymptotically exact.

In Section 3.2, it shows that the ISCR operator  $R_h$  has linearity, global boundedness and best approximation. In addition, it is a local gradient recovery operator. Hence, the ISCR operator  $R_h$  satisfies the conditions (I) and (II). Now we just need to consider that  $R_h$  satisfies the condition (III).

The supercloseness result has been proved in [23] as follows.

**Lemma 4.1.** *Let  $u$  be the exact solution of (1)-(2),  $u_h$  be the PPIFE solution of (8) generated with  $\gamma = 1$  on a Cartesian mesh  $\mathcal{T}_h$  and  $u_I$  be the linear interpolation of  $u$  in  $V_{h,0}$ . Given any  $u \in H^1(\Omega) \cap H^3(\Omega^+ \cup \Omega^-) \cap W^{2,\infty}(\Omega^+ \cup \Omega^-)$ , then*

$$(58) \quad a_h(u - u_I, v_h) \leq Ch^{\frac{3}{2}}(\|u\|_{3,\Omega^+ \cup \Omega^-} + \|u\|_{2,\infty,\Omega^+ \cup \Omega^-})\|v_h\|_h, \quad \forall v_h \in V_{h,0},$$

and

$$(59) \quad \|u_I - u_h\|_h \leq Ch^{\frac{3}{2}}(\|u\|_{3,\Omega^+ \cup \Omega^-} + \|u\|_{2,\infty,\Omega^+ \cup \Omega^-}),$$

where  $C$  is a constant independent of the mesh size  $h$  and the interface location.

Based on the above supercloseness results, we prove that the recovery gradient of PPIFE solution superconverges to the exact gradient.

**Theorem 4.1.** *Let  $R_h$  be the ISCR gradient recovery operator,  $u$  be the exact solution of (1)-(2) and  $u_h$  be the PPIFE solution of (8) generated with  $\gamma = 1$  on a Cartesian mesh  $\mathcal{T}_h$ . Given any  $u \in H^1(\Omega) \cap H^3(\Omega^+ \cup \Omega^-) \cap W^{2,\infty}(\Omega^+ \cup \Omega^-)$ , then*

$$(60) \quad \|\nabla u - R_h u_h\|_{0,\Omega} \leq Ch^{\frac{3}{2}}(\|u\|_{3,\Omega^+ \cup \Omega^-} + \|u\|_{2,\infty,\Omega^+ \cup \Omega^-}),$$

where  $C$  is a constant independent of the mesh size  $h$  and the interface location.

*Proof.* The boundedness (45) and the triangle inequality imply that

$$(61) \quad \|\nabla u - R_h u_h\|_{0,\Omega} \leq \|\nabla u - R_h u_I\|_{0,\Omega} + \|R_h u_I - R_h u_h\|_{0,\Omega} := I_1 + I_2.$$

According to Theorem 3.1, we have

$$(62) \quad I_1 \leq Ch^2(\|u\|_{3,\Omega^+ \cup \Omega^-} + \|u\|_{2,\infty,\Omega^+ \cup \Omega^-}).$$

By the definition of ISCR recovery operator, we get

$$(63) \quad I_2 = \|R_h(u_I - u_h)\|_{0,\Omega} \leq \|G_h^+ E_h(u_I - u_h)\|_{0,\Omega_h^+} + \|G_h^- E_h(u_I - u_h)\|_{0,\Omega_h^-}.$$

Notice that  $G_h^+$  and  $G_h^-$  are the standard SCR gradient recovery operator, then

$$\begin{aligned}
& \|G_h^+ E_h(u_I - u_h)\|_{0,\Omega_h^+} + \|G_h^- E_h(u_I - u_h)\|_{0,\Omega_h^-} \\
& \leq C \left( |E_h(u_I - u_h)|_{1,\Omega_h^+} + |E_h(u_I - u_h)|_{1,\Omega_h^-} \right) \\
(64) \quad & \leq C |E_h(u_I - u_h)|_{1,\Omega} \\
& \leq C |u_I - u_h|_{1,\Omega} \\
& \leq Ch^{\frac{3}{2}} (\|u\|_{3,\Omega \cup \Omega^-} + \|u\|_{2,\infty,\Omega \cup \Omega^-}),
\end{aligned}$$

where we use the boundedness of the standard SCR operator  $G_h^\pm$  in the first inequality, lemma 3.3 in the three inequality, and lemma 4.1 in the last inequality. Combining (61)-(64), we completes the proof of Theorem 4.1.  $\square$

With the superconvergence result above, we show that the ISCR-based error estimator is asymptotically exact.

**Theorem 4.2.** *In the hypotheses of Theorem 4.1. If there exist a constant  $C(u) > 0$ , such that*

$$(65) \quad \|\nabla u - \nabla u_h\|_{0,\Omega} \geq C(u)h.$$

Then, it holds that

$$(66) \quad \left| \frac{\eta_h}{\|\beta^{1/2} \nabla(u - u_h)\|_{0,\Omega}} - 1 \right| \leq Ch^{\frac{1}{2}}.$$

*Proof.* From the triangle inequality and Theorem 4.1, we have

$$\begin{aligned}
& \left| \|\beta^{1/2}(R_h u_h - \nabla u_h)\|_{0,\Omega} - \|\beta^{1/2} \nabla(u - u_h)\|_{0,\Omega} \right| \\
(67) \quad & \leq \|\beta^{1/2}(R_h u_h - \nabla u)\|_{0,\Omega} \\
& \leq Ch^{\frac{3}{2}} (\|u\|_{3,\Omega \cup \Omega^-} + \|u\|_{2,\infty,\Omega \cup \Omega^-}).
\end{aligned}$$

Therefore,

$$\begin{aligned}
(68) \quad & \left| \frac{\eta_h}{\|\beta^{1/2} \nabla(u - u_h)\|_{0,\Omega}} - 1 \right| \leq \left| \frac{\|\beta^{1/2}(R_h u_h - \nabla u_h)\|_{0,\Omega} - \|\beta^{1/2} \nabla(u - u_h)\|_{0,\Omega}}{\|\beta^{1/2} \nabla(u - u_h)\|_{0,\Omega}} \right| \\
& \leq \frac{Ch^{\frac{3}{2}} (\|u\|_{3,\Omega \cup \Omega^-} + \|u\|_{2,\infty,\Omega \cup \Omega^-})}{\min(\beta^+, \beta^-)c(u)h} \leq Ch^{\frac{1}{2}}.
\end{aligned}$$

This complete the proof.  $\square$

## 5. Numerical Experiments

In this section, we present some numerical examples to illustrate the superconvergence of the ISCR method, and show adaptive algorithm using the ISCR-based error estimator is reliable and efficient. We also demonstrate the effectiveness of this method by numerical comparison with the standard SCR method. For simplicity, we adopt the following error norms in all the examples:

$$De := \|u - u_h\|_{1,\Omega}, \quad D^i e := \|\nabla u - R_h u_h\|_{0,\Omega}, \quad D^s e := \|\nabla u - S_h u_h\|_{0,\Omega},$$

$$D^h e := \|\nabla u - H_h u_h\|_{0,\Omega}, \quad D^g e := \|\nabla u - G_h u_h\|_{0,\Omega}.$$

Our adaptive algorithm follows the standard procedure:

$$\text{Solve} \rightarrow \text{Estimate} \rightarrow \text{Remark} \rightarrow \text{Refine}.$$

We solve the elliptic interface problem using the PPIFE methods in (8), then estimate the ISCR-based error indicator  $\eta_T$  defined in (53) on each element. Mark the elements with the maximum marking strategy, i.e., mark all elements  $T^*$  such that

$$\eta_{T^*} \geq \theta \max_{T \in \mathcal{T}_h} \eta_T, \quad \theta \in (0, 1).$$

Finally, we refine the marked elements by newest vertex bisection.

**5.1. Example 1.** In first example, we consider the elliptic interface problem with a smooth circular interface curve [6, 23, 24]. Assume the interface  $\Gamma$  is a circle centered at origin with radius  $r_0 = \frac{\pi}{6.28}$ , and separates the domain  $\Omega = [-1, 1]^2$  into two subdomains  $\Omega^+ = \{(x, y) : x^2 + y^2 > r_0^2\}$  and  $\Omega^- = \{(x, y) : x^2 + y^2 < r_0^2\}$ . The function  $f$  is chosen to fit the following exact solution

$$(69) \quad u(z) = \begin{cases} \frac{r^p}{\beta^+} + \left(\frac{1}{\beta^-} - \frac{1}{\beta^+}\right) r_0^p, & \text{if } z \in \Omega^+, \\ \frac{r^p}{\beta^-}, & \text{if } z \in \Omega^-, \end{cases}$$

where  $r = \sqrt{x^2 + y^2}$  and  $p = 3$ .

Here we take  $\frac{\beta^+}{\beta^-} = \frac{1}{10}, \frac{1}{100}, \frac{1}{1000}, \frac{10}{1}, \frac{100}{1}, \frac{1000}{1}$  in Tables 1 and Tables 2. As we see clearly that  $H^1$ -semi error ( $De$ ) reach the optimal convergence rate for different jump ratios. For the convergence rate of gradients, ISCR ( $D^i e$ ), ISCR-AA ( $D^s e$ ) and ISCR-AH ( $D^h e$ ) superconverges at the order of  $O(h^{1.5})$ , but the standard SCR ( $D^g e$ ) is about  $O(h^{0.5})$  convergence rate. One also notice that  $D^i e$ ,  $D^s e$  and  $D^h e$  have similar superconvergence results, but the error of  $D^i e$  is slightly smaller than that of  $D^s e$  and  $D^h e$ .

In Figure 5, we plot the meshes generated by the uniform PPIFE and adaptive PPIFE methods with the jump ratio  $\beta^+/\beta^- = 100/1$ , where Figure 5 (a) has a similar number of elements and degrees of freedom (DOF) as Figure 5 (b). Compared with the uniform mesh, it can be observed from Figure 5 (b) that there is mainly mesh refinement around the interface for the adaptive PPIFE methods.

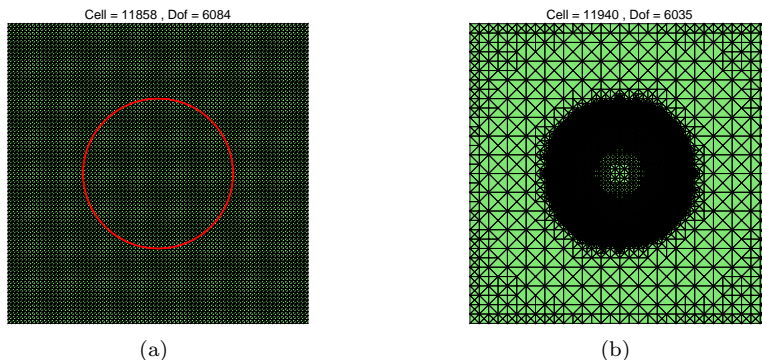


FIGURE 5. The mesh generated by the uniform PPIFE and adaptive PPIFE methods with the jump ratio  $\beta^+/\beta^- = 100/1$  for Example 5.1. (a) Uniform mesh; (b) Adaptive mesh.

TABLE 1. Numerical results for Examples 5.1 with  $\beta^+/\beta^- = 1/10$ ,  $\beta^+/\beta^- = 1/100$  and  $\beta^+/\beta^- = 1/1000$  using PPIFE and four gradient recovery methods.

$Dof$	$\frac{\beta^+}{\beta^-} = \frac{1}{10}$	Order	$\frac{\beta^+}{\beta^-} = \frac{1}{100}$	Order	$\frac{\beta^+}{\beta^-} = \frac{1}{1000}$	Order
PPIFE methods in $\ u - u_h\ _{1,\Omega}$						
81	$7.9735e - 01$	—	$8.0201e - 01$	—	$8.0214e - 01$	—
289	$3.9971e - 01$	0.9963	$4.0107e - 01$	0.9998	$4.0108e - 01$	0.9999
1089	$2.0016e - 01$	0.9978	$2.0060e - 01$	0.9995	$2.0062e - 01$	0.9994
4225	$1.0007e - 01$	1.0001	$1.0019e - 01$	1.0015	$1.0020e - 01$	1.0016
16641	$5.0062e - 02$	0.9993	$5.0098e - 02$	0.9999	$5.0100e - 02$	1.0000
ISCR method in $\ \nabla u - R_h u_h\ _{0,\Omega}$						
81	$1.0836e + 00$	—	$1.0854e + 00$	—	$1.0860e + 00$	—
289	$4.3127e - 01$	1.3292	$4.3233e - 01$	1.3281	$4.3251e - 01$	1.3282
1089	$1.6152e - 01$	1.4169	$1.6203e - 01$	1.4159	$1.6209e - 01$	1.4159
4225	$5.8675e - 02$	1.4609	$5.8927e - 02$	1.4592	$5.8953e - 02$	1.4592
16641	$2.1109e - 02$	1.4749	$2.1212e - 02$	1.4741	$2.1220e - 02$	1.4741
ISCR-AA method in $\ \nabla u - S_h u_h\ _{0,\Omega}$						
81	$1.0852e + 00$	—	$1.0864e + 00$	—	$1.0869e + 00$	—
289	$4.3167e - 01$	1.3299	$4.3258e - 01$	1.3285	$4.3275e - 01$	1.3286
1089	$1.6162e - 01$	1.4173	$1.6208e - 01$	1.4162	$1.6214e - 01$	1.4163
4225	$5.8706e - 02$	1.4610	$5.8948e - 02$	1.4592	$5.8973e - 02$	1.4591
16641	$2.1113e - 02$	1.4754	$2.1213e - 02$	1.4745	$2.1222e - 02$	1.4745
ISCR-AH method in $\ \nabla u - H_h u_h\ _{0,\Omega}$						
81	$1.0857e + 00$	—	$1.0875e + 00$	—	$1.0880e + 00$	—
289	$4.3114e - 01$	1.3324	$4.3234e - 01$	1.3308	$4.3252e - 01$	1.3309
1089	$1.6151e - 01$	1.4165	$1.6210e - 01$	1.4153	$1.6216e - 01$	1.4153
4225	$5.8666e - 02$	1.4610	$5.8961e - 02$	1.4590	$5.8991e - 02$	1.4589
16641	$2.1119e - 02$	1.4740	$2.1221e - 02$	1.4743	$2.1229e - 02$	1.4744
SCR method in $\ \nabla u - G_h u_h\ _{0,\Omega}$						
81	$1.1515e + 00$	—	$1.1819e + 00$	—	$1.1853e + 00$	—
289	$4.4875e - 01$	1.3595	$4.5606e - 01$	1.3738	$4.5675e - 01$	1.3757
1089	$1.8094e - 01$	1.3104	$1.8589e - 01$	1.2948	$1.8634e - 01$	1.2934
4225	$8.3518e - 02$	1.1154	$8.8261e - 02$	1.0746	$8.8712e - 02$	1.0708
16641	$4.7320e - 02$	0.8196	$5.1316e - 02$	0.7824	$5.1707e - 02$	0.7788
66049	$3.1120e - 02$	0.6046	$3.4117e - 02$	0.5889	$3.4412e - 02$	0.5874

Figure 6 and 7 show the numerical solutions and the recovered gradient. Figure 8 describes the error surfaces of the uniform and adaptive PPIFE methods with similar DOFs, respectively. We can observe that the error is obviously reduced for the adaptive solution, which can also be clearly seen from Figure 9.

In Figure 9, we present the convergence of these two methods and the ISCR-based error estimator for the adaptive PPIFE methods. As shown in the figure, the error of adaptive PPIFE methods is significantly less than that of uniform PPIFE methods, and the slopes of uniform and adaptive PPIFE methods  $\log(\text{DOF})-\log(\text{De})$  are very close to  $-0.5$  and  $-0.7$ , respectively. Hence, the application of adaptive mesh refinement is more efficient for interface problems with moderate jump ratios. We will also explain that it is also effective for the case of large jump ratios. And we

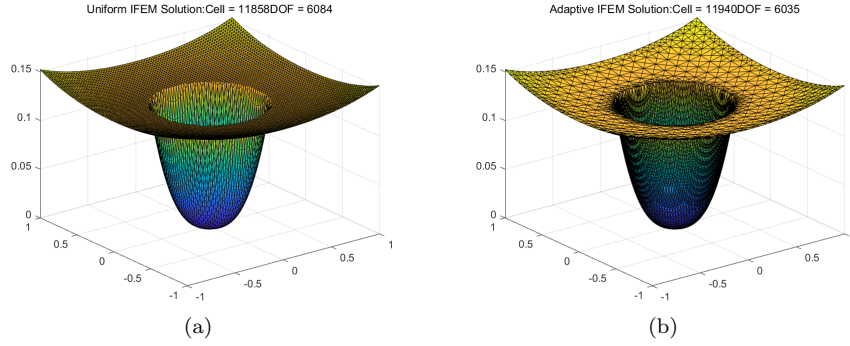


FIGURE 6. Numerical solutions of uniform and adaptive PPIFE methods with similar DOFs and  $\beta^+/\beta^- = 100/1$  for Example 5.1. (a) Numerical solutions of uniform PPIFE methods; (b) Numerical solutions of adaptive PPIFE methods.

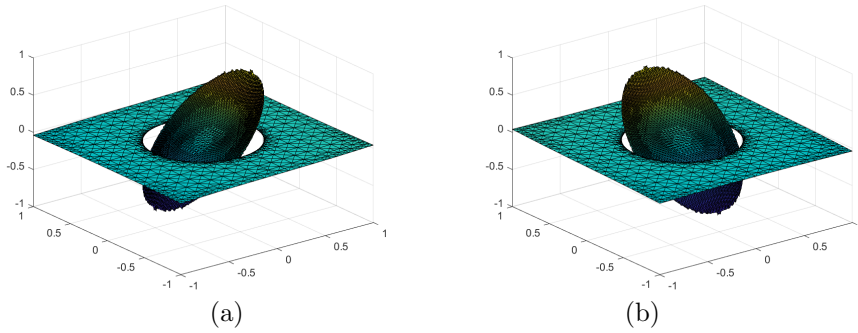


FIGURE 7. Recoverd gradient with  $\beta^+ = 100, \beta^- = 1$  for Example 5.1. (a) x-component; (b) y-component.

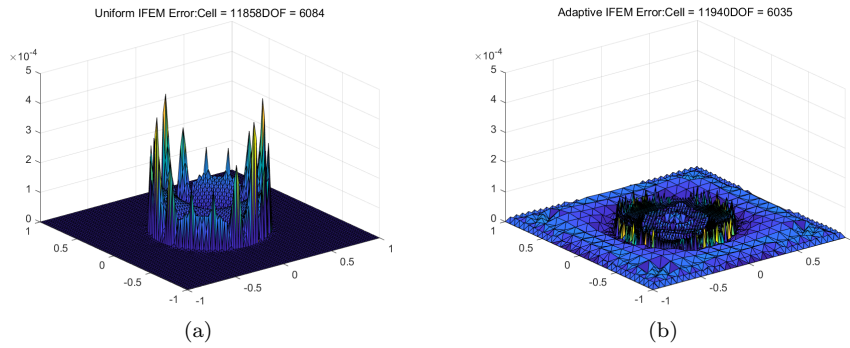


FIGURE 8. Errors of uniform and adaptive PPIFE methods with similar DOFs and  $\beta^+/\beta^- = 100/1$  for Example 5.1. (a) Errors of uniform PPIFE methods; (b) Errors of adaptive PPIFE methods.

TABLE 2. Numerical results for Examples 5.1 with  $\beta^+/\beta^- = 10/1$ ,  $\beta^+/\beta^- = 100/1$  and  $\beta^+/\beta^- = 1000/1$  using PPIFE and four gradient recovery methods.

<i>Dof</i>	$\frac{\beta^+}{\beta^-} = \frac{10}{1}$	Order	$\frac{\beta^+}{\beta^-} = \frac{100}{1}$	Order	$\frac{\beta^+}{\beta^-} = \frac{1000}{1}$	Order
PPIFE methods in $\ u - u_h\ _{1,\Omega}$						
81	$1.7490e - 01$	—	$1.6137e - 01$	—	$1.6029e - 01$	—
289	$8.7314e - 02$	1.0023	$8.1182e - 02$	0.9911	$7.8824e - 02$	1.0240
1089	$4.3903e - 02$	0.9919	$4.0441e - 02$	1.0053	$3.9629e - 02$	0.9921
4225	$2.1828e - 02$	1.0082	$1.9763e - 02$	1.0330	$1.9538e - 02$	1.0203
16641	$1.1008e - 02$	0.9876	$9.9169e - 03$	0.9949	$9.8510e - 03$	0.9879
ISCR method in $\ \nabla u - R_h u_h\ _{0,\Omega}$						
81	$1.6184e - 01$	—	$1.3701e - 01$	—	$1.8413e - 01$	—
289	$6.6367e - 02$	1.2860	$5.8274e - 02$	1.2334	$7.3164e - 02$	1.3315
1089	$2.5385e - 02$	1.3865	$2.3486e - 02$	1.3111	$2.7625e - 02$	1.4052
4225	$8.9172e - 03$	1.5093	$8.2893e - 03$	1.5025	$8.6265e - 03$	1.6791
16641	$3.3154e - 03$	1.4274	$3.0704e - 03$	1.4328	$2.9590e - 03$	1.5437
ISCR-AA method in $\ \nabla u - S_h u_h\ _{0,\Omega}$						
81	$1.6682e - 01$	—	$1.4271e - 01$	—	$1.8350e - 01$	—
289	$6.8006e - 02$	1.2945	$6.0272e - 02$	1.2435	$7.2129e - 02$	1.3472
1089	$2.5790e - 02$	1.3988	$2.3780e - 02$	1.3417	$2.6770e - 02$	1.4300
4225	$9.0391e - 03$	1.5126	$8.3087e - 03$	1.5171	$8.4450e - 03$	1.6644
16641	$3.3659e - 03$	1.4252	$3.1185e - 03$	1.4138	$5.0137e - 03$	1.4866
ISCR-AH method in $\ \nabla u - H_h u_h\ _{0,\Omega}$						
81	$1.7515e - 01$	—	$1.5994e - 01$	—	$2.5731e - 01$	—
289	$6.7787e - 02$	1.3695	$6.4129e - 02$	1.3185	$1.0393e - 01$	1.3079
1089	$2.5815e - 02$	1.3928	$2.6367e - 02$	1.2822	$3.8395e - 02$	1.4366
4225	$8.9822e - 03$	1.5231	$9.2292e - 03$	1.5145	$1.0804e - 02$	1.8294
16641	$3.3205e - 03$	1.4357	$3.0751e - 03$	1.5856	$2.9695e - 03$	1.8632
SCR method in $\ \nabla u - G_h u_h\ _{0,\Omega}$						
81	$3.7670e - 01$	—	$3.8620e - 01$	—	$5.9636e - 01$	—
289	$1.5683e - 01$	1.2642	$1.6631e - 01$	1.2154	$2.9679e - 01$	1.0067
1089	$9.3354e - 02$	0.7484	$1.0216e - 01$	0.7031	$1.3535e - 01$	1.1327
4225	$6.2711e - 02$	0.5740	$6.8909e - 02$	0.5680	$7.5100e - 02$	0.8498
16641	$4.3539e - 02$	0.5264	$4.7720e - 02$	0.5301	$4.8276e - 02$	0.6375
66049	$3.0574e - 02$	0.5100	$3.3581e - 02$	0.5069	$3.3914e - 02$	0.5094

can also see that although the rate of the ISCR-based error estimator is slightly lower than the theoretical order  $O(h^{1.5})$  due to the complexity of adaptive mesh, the error estimator is still effective in guiding mesh refinement and is asymptotically exact.

We also test the case with a large jump ratio  $\beta^+/\beta^- = 1000/1$ . Figure 10 (a) shows that the mesh of the adaptive PPIFE methods is effectively refined in regions near the interface. In Figure 10 (b), we note that the slope of uniform and adaptive PPIFE methods is consistent with Figure 9, which illustrates that the adaptive PPIFE methods are also more effective than the uniform PPIFE methods for the case of large jump ratios. And the ISCR-based error estimator has superconvergence results and asymptotically exactness.

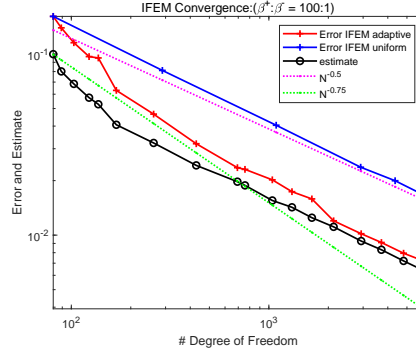


FIGURE 9. Convergence of uniform PPIFE and adaptive PPIFE methods with  $\beta^+/\beta^- = 100/1$  for Example 5.1.

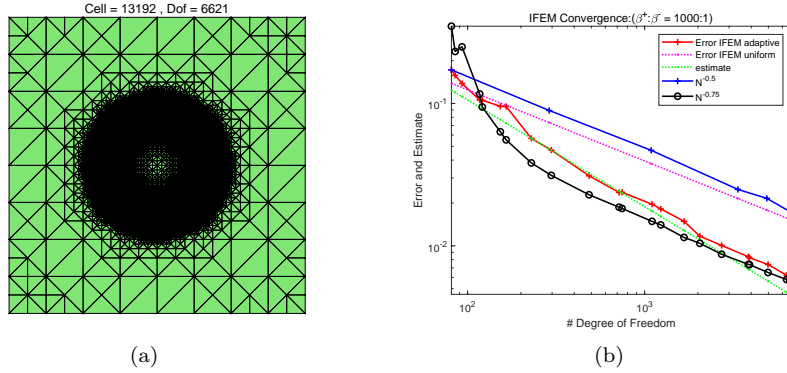


FIGURE 10. Adaptive mesh for PPIFE methods and convergence of uniform and adaptive PPIFE methods with  $\beta^+/\beta^- = 1000/1$  for Example 5.1. (a) Adaptive mesh; (b) Convergence.

The numerical solutions and the error surfaces on the uniform and adaptive meshes with similar DOFs are described in Figure 11 and 12, respectively. Again, we can see that the error of adaptive PPIFE methods is less than the error of uniform PPIFE methods with similar degrees of freedom.

**5.2. Example 2.** In this example, we consider the elliptic interface problem with a more complicated interface curve [35]. Let  $\Omega = [-1, 1] \times [-1, 1]$ , and the interface is the zero level set of the following function

$$\phi(x, y) = (x^2 + y^2)^2 \left( 1 + 0.4 \sin \left( 6 \arctan \left( \frac{y}{x} \right) \right) \right) - 0.3.$$

The two subdomains are defined as  $\Omega^+ = \{(x, y) : \phi(x, y) > 0\}$  and  $\Omega^- = \{(x, y) : \phi(x, y) < 0\}$ . The right hand function  $f$  is selected to match the exact solution

$$u(z) = \begin{cases} \frac{1}{\beta^+} \phi(x, y), & \text{if } z \in \Omega^+, \\ \frac{1}{\beta^-} \phi(x, y), & \text{if } z \in \Omega^-. \end{cases}$$

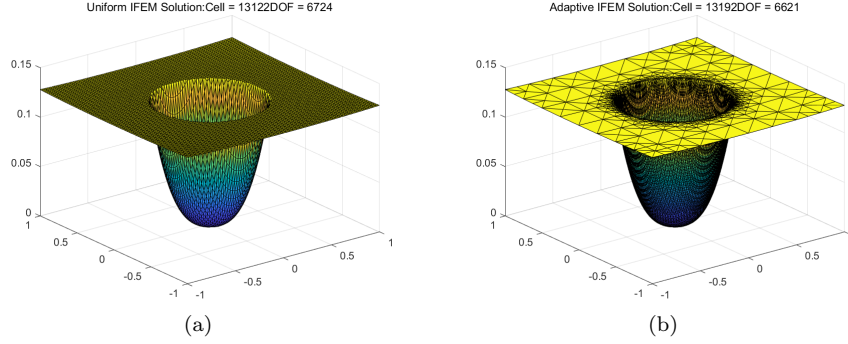


FIGURE 11. Numerical solutions of uniform and adaptive PPIFE methods with similar DOFs and  $\beta^+/\beta^- = 1000/1$  for Example 5.1. (a) Numerical solutions of uniform PPIFE methods; (b) Numerical solutions of adaptive PPIFE methods.

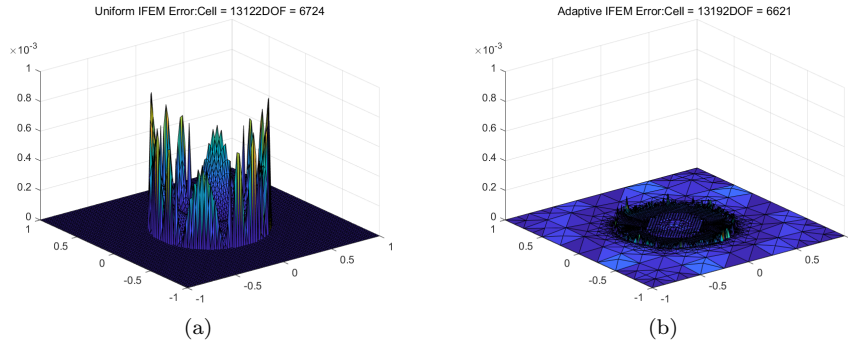


FIGURE 12. Errors of uniform and adaptive PPIFE methods with similar DOFs and  $\beta^+/\beta^- = 1000/1$  for Example 5.1. (a) Errors of uniform PPIFE methods; (b) Errors of adaptive PPIFE methods.

For this example, we choose the same jump ratios as in the Example 5.1. Because of the complexity of the interface shape, we start with a  $16 \times 16$  Cartesian triangular mesh. Tables 3 and 4 show the corresponding numerical results, from which one can see that  $H^1$ -semi error ( $De$ ) of the PPIFE numerical solution decays at an optimal rate of  $O(h)$ . ISCR ( $D^i e$ ), ISCR-AA ( $D^s e$ ) and ISCR-AH ( $D^h e$ ) have an  $O(h^{1.5})$  superconvergence, which is consistent with Theorem 4.1. However, the standard SCR ( $D^g e$ ) does not converge since the exact solution is smooth only on each subdomain. We can also note that the error of  $D^i e$  is slightly less than that of  $D^s e$  and  $D^h e$ .

We present the adaptive mesh and the convergence with  $\beta^+/\beta^- = 100/1$  in Figure 13. The plot on the left shows that the interface is petal-shaped, and the mesh refinement is concentrated near the interface. Figure 13 (b) illustrates that the uniform and adaptive PPIFE errors have  $O(h)$  and  $O(h^{1.4})$  convergence rates, respectively. And although the order of the ISCR-based error estimator is slightly lower than that of the theoretical, it still achieves good results. Figure 14 and

TABLE 3. Numerical results for Examples 5.2 with  $\beta^+/\beta^- = 1/10$ ,  $\beta^+/\beta^- = 1/100$  and  $\beta^+/\beta^- = 1/1000$  using PPIFE and four gradient recovery methods.

<i>Dof</i>	$\frac{\beta^+}{\beta^-} = \frac{1}{10}$	Order	$\frac{\beta^+}{\beta^-} = \frac{1}{100}$	Order	$\frac{\beta^+}{\beta^-} = \frac{1}{1000}$	Order
PPIFE method in $\ u - u_h\ _{1,\Omega}$						
289	$9.7177e - 01$	-	$1.0573e + 00$	-	$1.1147e + 00$	-
1089	$4.8746e - 01$	0.9953	$4.9544e - 01$	1.0936	$5.3504e - 01$	1.0589
4225	$2.4455e - 01$	0.9952	$2.4584e - 01$	1.0110	$2.4896e - 01$	1.1038
16641	$1.2222e - 01$	1.0007	$1.2275e - 01$	1.0020	$1.2431e - 01$	1.0020
ISCR method in $\ \nabla u - R_h u_h\ _{0,\Omega}$						
289	$1.1162e + 00$	-	$1.1493e + 00$	-	$1.1533e + 00$	-
1089	$4.2468e - 01$	1.3942	$4.2762e - 01$	1.4264	$4.4184e - 01$	1.3842
4225	$1.5577e - 01$	1.4470	$1.5692e - 01$	1.4463	$1.5820e - 01$	1.4818
16641	$5.6097e - 02$	1.4734	$5.6658e - 02$	1.4697	$5.8180e - 02$	1.4432
ISCR-AA method in $\ \nabla u - S_h u_h\ _{0,\Omega}$						
289	$1.1170e + 00$	-	$1.1493e + 00$	-	$1.1529e + 00$	-
1089	$4.2519e - 01$	1.3935	$4.2798e - 01$	1.4251	$4.4246e - 01$	1.3816
4225	$1.5588e - 01$	1.4477	$1.5708e - 01$	1.4460	$1.5842e - 01$	1.4818
16641	$5.6131e - 02$	1.4735	$5.6692e - 02$	1.4703	$5.8193e - 02$	1.4448
ISCR-AH method in $\ \nabla u - H_h u_h\ _{0,\Omega}$						
289	$1.1166e + 00$	-	$1.1499e + 00$	-	$1.1538e + 00$	-
1089	$4.2465e - 01$	1.3948	$4.2766e - 01$	1.4270	$4.4153e - 01$	1.3858
4225	$1.5594e - 01$	1.4453	$1.5705e - 01$	1.4452	$1.5827e - 01$	1.4801
16641	$5.6143e - 02$	1.4738	$5.6722e - 02$	1.4692	$5.8397e - 02$	1.4384
SCR method in $\ \nabla u - G_h u_h\ _{0,\Omega}$						
289	$1.1487e + 00$	-	$1.1905e + 00$	-	$1.1966e + 00$	-
1089	$4.8732e - 01$	1.2371	$5.0346e - 01$	1.2416	$5.1821e - 01$	1.2073
4225	$2.3573e - 01$	1.0478	$2.5065e - 01$	1.0062	$2.5330e - 01$	1.0327
16641	$1.3843e - 01$	0.7680	$1.5081e - 01$	0.7329	$1.5342e - 01$	0.7234
66049	$9.2837e - 02$	0.5764	$1.0197e - 01$	0.5646	$1.0317e - 01$	0.5725

Figure 15 indicate that the error mainly comes from the interface elements, and the adaptive PPIFE methods can significantly reduce the error.

We also test the large jump case by choosing  $\beta^+ = 1000$  and  $\beta^- = 1$ . Figure 16 plots an adaptively refined mesh and gives the numerical convergence rates. It shows clearly from Figure 16 (a) that the recovery-based a posteriori error estimator successfully directs the mesh refinement around the interface without introducing any over-refinement. However, the a posteriori error estimator based on standard gradient recovery operators exists the over-refinement problem discussed in [31]. One can again observe from Figure 16 (b), the optimal rate decay for the uniform PPIFE numerical errors, and the superconvergence for the adaptive PPIFE numerical errors and estimator. And Figure 17 and 18 also illustrate the good performance of the ISCR-based error estimator for the partially penalized IFE methods.

**5.3. Example 3.** In this example, we consider the interface problem where the exact solution has singularity [24, 36]. Let  $\Omega = [-1, 1] \times [-1, 1]$ , and the interface  $\Gamma$  be an ellipse centered at  $(x_0, y_0) = (0, 0)$  with semi-axes  $a = \frac{\pi}{6.28}$ ,  $b = \frac{3}{2}a$ . The

TABLE 4. Numerical results for Examples 5.2 with  $\beta^+/\beta^- = 10/1$ ,  $\beta^+/\beta^- = 100/1$  and  $\beta^+/\beta^- = 1000/1$  using PPIFE and four gradient recovery methods.

<i>Dof</i>	$\frac{\beta^+}{\beta^-} = \frac{10}{1}$	Order	$\frac{\beta^+}{\beta^-} = \frac{100}{1}$	Order	$\frac{\beta^+}{\beta^-} = \frac{1000}{1}$	Order
PPIFE method in $\ u - u_h\ _{1,\Omega}$						
289	$3.1103e - 01$	-	$2.9320e - 01$	-	$3.1635e - 01$	-
1089	$1.6164e - 01$	0.9442	$1.5509e - 01$	0.9187	$1.6215e - 01$	0.9642
4225	$8.1971e - 02$	0.9796	$7.8679e - 02$	0.9791	$7.9796e - 02$	1.0229
16641	$4.0751e - 02$	1.0083	$3.8959e - 02$	1.0140	$3.9332e - 02$	1.0206
ISCR method in $\ \nabla u - R_h u_h\ _{0,\Omega}$						
289	$2.1753e - 01$	-	$2.2978e - 01$	-	$2.5149e - 01$	-
1089	$7.3522e - 02$	1.5650	$8.1065e - 02$	1.5031	$9.8192e - 02$	1.3568
4225	$2.9299e - 02$	1.3273	$3.2506e - 02$	1.3184	$3.5337e - 02$	1.4744
16641	$1.0606e - 02$	1.4660	$1.1950e - 02$	1.4436	$1.3406e - 02$	1.3983
ISCR-AA method in $\ \nabla u - S_h u_h\ _{0,\Omega}$						
289	$2.1352e - 01$	-	$1.9839e - 01$	-	$2.2476e - 01$	-
1089	$8.5129e - 02$	1.3267	$8.1655e - 02$	1.2807	$9.6041e - 02$	1.2267
4225	$3.3648e - 02$	1.3391	$3.3105e - 02$	1.3025	$3.5607e - 02$	1.4315
16641	$1.2154e - 02$	1.4691	$1.2130e - 02$	1.4485	$1.3417e - 02$	1.4081
ISCR-AH method in $\ \nabla u - H_h u_h\ _{0,\Omega}$						
289	$2.1218e - 01$	-	$1.9545e - 01$	-	$2.2409e - 01$	-
1089	$8.6099e - 02$	1.3012	$8.4046e - 02$	1.2175	$1.0981e - 01$	1.0290
4225	$3.3225e - 02$	1.3737	$3.2590e - 02$	1.3668	$3.5546e - 02$	1.6272
16641	$1.1977e - 02$	1.4720	$1.1987e - 02$	1.4430	$1.3639e - 02$	1.3819
SCR method in $\ \nabla u - G_h u_h\ _{0,\Omega}$						
289	$4.3123e - 01$	-	$4.4273e - 01$	-	$4.4976e - 01$	-
1089	$2.7652e - 01$	0.6411	$2.9888e - 01$	0.5669	$3.0839e - 01$	0.5444
4225	$1.8779e - 01$	0.5583	$2.0486e - 01$	0.5449	$2.0625e - 01$	0.5804
16641	$1.3122e - 01$	0.5171	$1.4347e - 01$	0.5139	$1.4461e - 01$	0.5122

interface separates the domain  $\Omega$  into two subdomains, denoted by  $\Omega^+$  and  $\Omega^-$  such that

$$\Omega^+ = \{(x, y) : r(x, y) > 1\} \quad \text{and} \quad \Omega^- = \{(x, y) : r(x, y) < 1\},$$

where

$$r(x, y) = \sqrt{\frac{(x - x_0)^2}{a^2} + \frac{(y - y_0)^2}{b^2}}.$$

The right hand function  $f$  is given by the exact solution

$$(70) \quad u(z) = \begin{cases} \frac{r^p}{\beta^+} + \frac{1}{\beta^-} - \frac{1}{\beta^+}, & \text{if } z \in \Omega^+, \\ \frac{r^p}{\beta^-}, & \text{if } z \in \Omega^-, \end{cases}$$

where  $p > 0$  is the regularity parameter.

We test the case when  $p = 0.5$  and  $\beta^+/\beta^- = 10^6/1$ . Note that the singularity of the exact solution at origin leads to the solution is merely in  $H^{1.5-\rho}(\Omega)$  for any  $\rho > 0$ . The adaptively refined mesh presented in Figure 19 (a) shows that

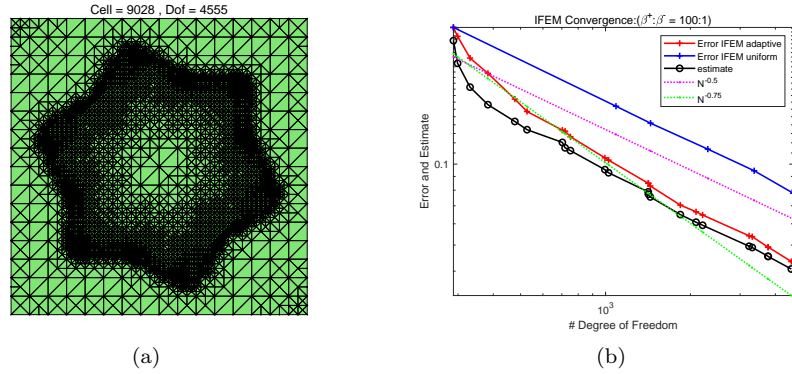


FIGURE 13. Adaptive mesh for PPIFE methods and convergence of uniform and adaptive PPIFE methods with  $\beta^+/\beta^- = 100/1$  for Example 5.2. (a) Adaptive mesh; (b) Convergence.

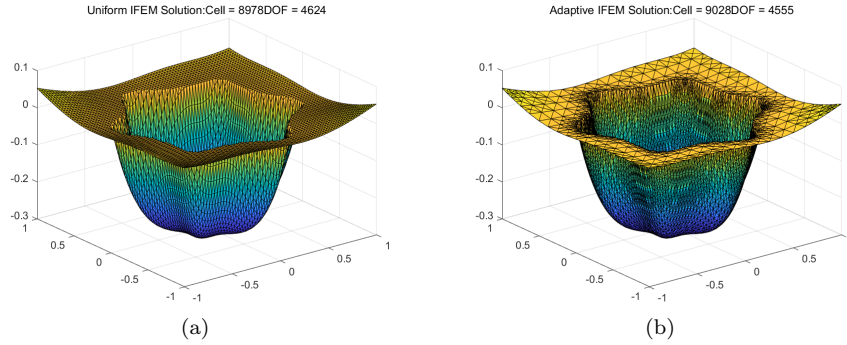


FIGURE 14. Numerical solutions of uniform and adaptive PPIFE methods with similar DOFs and  $\beta^+/\beta^- = 100/1$  for Example 5.2. (a) Numerical solutions of uniform PPIFE methods; (b) Numerical solutions of adaptive PPIFE methods.

the refinement is around the interface and the origin where the exact solution is singular. Figure 19 (b) displays the numerical convergence rates. As shown in the plot, the adaptive PPIFE methods are far more accurate than the uniform PPIFE methods with similar DOFs. Moreover, we can draw similar conclusions as previous about the convergence of error and estimator for the adaptive PPIFE methods. However, the uniform PPIFE methods fail to converge optimally due to the singularity of the solution.

In Figure 20 and 21, the numerical solutions and the error surfaces on the uniform and adaptive meshes are reported, respectively. Obviously, the numerical solution obtained by the adaptive PPIFE methods can accurately resolve the behavior of the exact solution at the singularity point, and the adaptive PPIFE methods can significantly reduce the error mainly from around the singular point.

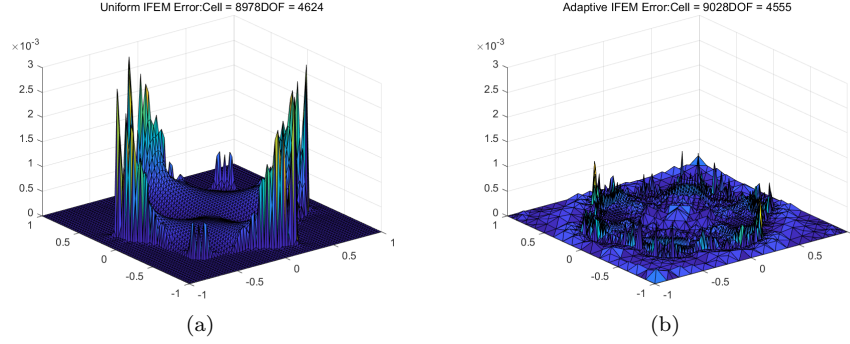


FIGURE 15. Errors of uniform and adaptive PPIFE methods with similar DOFs and  $\beta^+/\beta^- = 100/1$  for Example 5.2. (a) Errors of uniform PPIFE methods; (b) Errors of adaptive PPIFE methods.

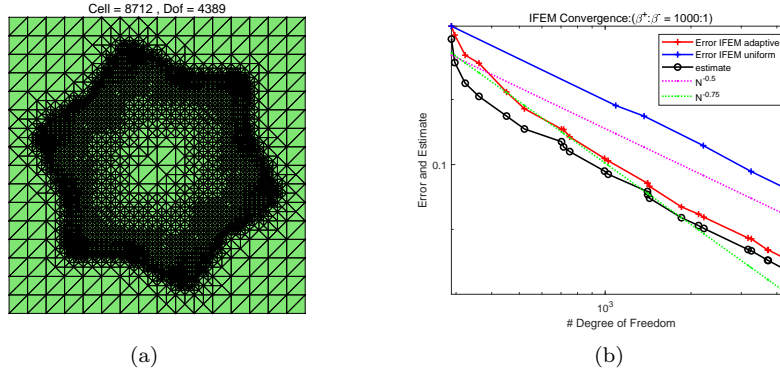


FIGURE 16. Adaptive mesh for PPIFE methods and convergence of uniform and adaptive PPIFE methods with  $\beta^+/\beta^- = 1000/1$  for Example 5.2. (a) Adaptive mesh; (b) Convergence.

### 6. Conclusion

In this paper, we have developed an immersed superconvergent cluster recovery method and a posteriori error estimation based on this method for elliptic interface problems solved by partially penalized immersed finite element methods. The proposed gradient recovery operator, which overcomes the shortcoming that the standard gradient recovery methods cannot obtain superconvergence results due to the low regularity of the solution at the interface, was proved to have linearity, boundedness, and consistent properties. The recovered gradient converges to the exact gradient at the superconvergent rate of  $O(h^{1.5})$ . We present several numerical examples to confirm our theoretical results and verify that the a posteriori error estimator is asymptotically exact for the adaptive algorithm. In our future work, we will consider a recovery-based a posteriori error estimate for immersed finite element methods to parabolic interface problems.

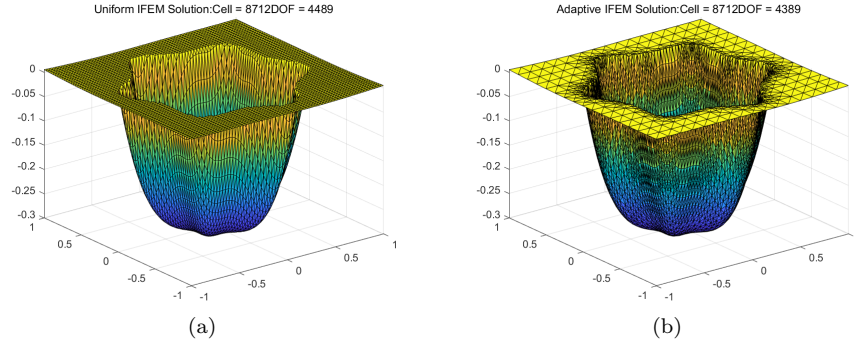


FIGURE 17. Numerical solutions of uniform and adaptive PPIFE methods with similar DOFs and  $\beta^+/\beta^- = 1000/1$  for Example 5.2. (a) Numerical solutions of uniform PPIFE methods; (b) Numerical solutions of adaptive PPIFE methods.

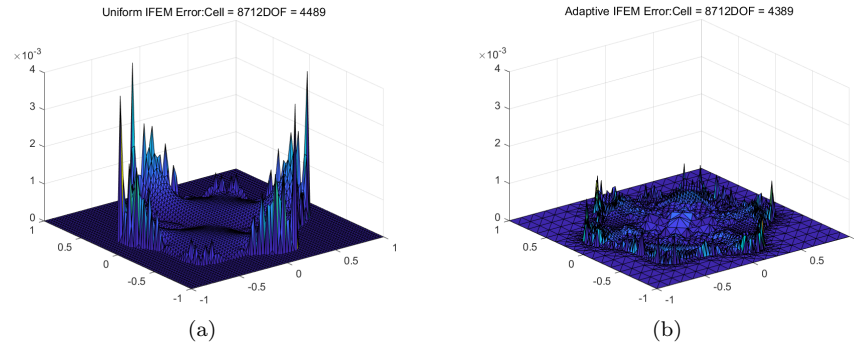


FIGURE 18. Errors of uniform and adaptive PPIFE methods with similar DOFs and  $\beta^+/\beta^- = 1000/1$  for Example 5.2. (a) Errors of uniform PPIFE methods; (b) Errors of adaptive PPIFE methods.

## Acknowledgments

This work is supported by the State Key Program of National Natural Science Foundation of China (11931003) and National Natural Science Foundation of China (41974133, 11971410).

## References

- [1] H. Wei, L. Chen, Y. Huang, B. Zheng, Adaptive mesh refinement and superconvergence for two-dimensional interface problems, *SIAM Journal on Scientific Computing* 36 (4) (2013) A1478–A1499.
- [2] L. Chen, H. Wei, M. Wen, An interface-fitted mesh generator and virtual element methods for elliptic interface problems, *Journal of Computational Physics* 334 (2017) 327–348.
- [3] Z. Chen, J. Zou, Finite element methods and their convergence for elliptic and parabolic interface problems, *Numerische Mathematik* 79 (2) (1998) 175–202.
- [4] Y. Chen, Q. Li, Y. Wang, Y. Huang, Two-grid methods of finite element solutions for semi-linear elliptic interface problems, *Numerical Algorithms* 84 (1) (2019) 307–330.

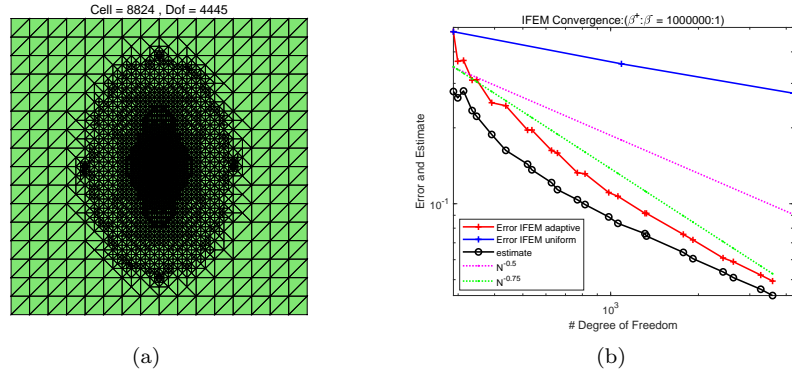


FIGURE 19. Adaptive mesh for PPIFE methods and convergence of uniform and adaptive PPIFE methods with  $\beta^+/\beta^- = 10^6/1$  for Example 5.3. (a) Adaptive mesh; (b) Convergence.

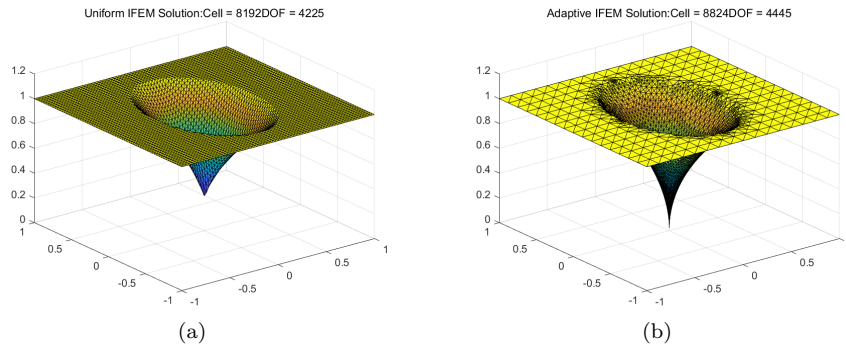


FIGURE 20. Numerical solutions of uniform and adaptive PPIFE methods with similar DOFs and  $\beta^+/\beta^- = 10^6/1$  for Example 5.3. (a) Numerical solutions of uniform PPIFE methods; (b) Numerical solutions of adaptive PPIFE methods.

[5] A. Hansbo, P. Hansbo, A finite element method for the simulation of strong and weak discontinuities in solid mechanics, *Computer Methods in Applied Mechanics and Engineering* 193 (33/35) (2004) 3523–3540.

[6] T. Lin, Y. Lin, X. Zhang, Partially penalized immersed finite element methods for elliptic interface problems, *SIAM Journal on Numerical Analysis* 53 (2) (2015) 1121–1144.

[7] Y. Wang, Y. Chen, Y. Huang, Y. Liu, Two-grid methods for semi-linear elliptic interface problems by immersed finite element methods, *Applied Mathematics and Mechanics* 40 (11) (2019) 1657–1676.

[8] J. H. Bramble, J. T. King, A finite element method for interface problems in domains with smooth boundaries and interfaces, *Advances in Computational Mathematics* 6 (1) (1996) 109–138.

[9] I. Babuška, The finite element method for elliptic equations with discontinuous coefficients, *Computing* 5 (3) (1970) 207–213.

[10] Z. Li, L. Tao, X. Wu, New cartesian grid methods for interface problems using the finite element formulation, *Numerische Mathematik* 96 (1) (2003) 61–98.

[11] Z. Li, The immersed interface method using a finite element formulation, *Appl. numer. math* 27 (3) (1998) 253–267.

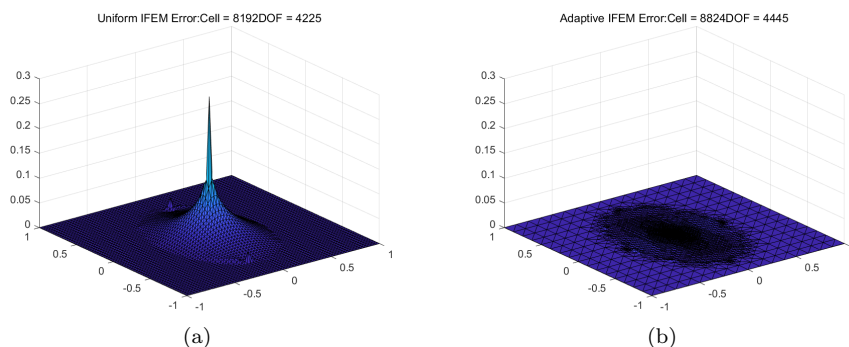


FIGURE 21. Errors of uniform and adaptive PPIFE methods with similar DOFs and  $\beta^+/\beta^- = 10^6/1$  for Example 5.3. (a) Errors of uniform PPIFE methods; (b) Errors of adaptive PPIFE methods.

- [12] Z. Li, T. Lin, Y. Lin, R. C. Rogers, An immersed finite element space and its approximation capability, *Numerical Methods for Partial Differential Equations* 20 (3) (2010) 338–367.
- [13] S. H. Chou, D. Y. Kwak, K. T. Wee, Optimal convergence analysis of an immersed interface finite element method, *Advances in Computational Mathematics* 33 (2) (2010) 149–168.
- [14] H. Ji, J. Chen, Z. Li, A symmetric and consistent immersed finite element method for interface problems, *Journal of Scientific Computing* 61 (3) (2014) 533–557.
- [15] T. Y. Hou, X. H. Wu, Y. Zhang, Removing the cell resonance error in the multiscale finite element method via a petrov-galerkin formulation, *Communications in Mathematical Sciences* 2 (2) (2004) 185–205.
- [16] R. Guo, T. Lin, Q. Zhuang, Improved error estimation for the partially penalized immersed finite element methods for elliptic interface problems, *International Journal of Numerical Analysis and Modeling* 16 (4) (2019) 575–589.
- [17] Y. Wang, Y. Chen, Y. Huang, A two-grid method for semi-linear elliptic interface problems by partially penalized immersed finite element methods, *Mathematics and Computers in Simulation* 169 (2020) 1–15.
- [18] H. Ji, Q. Zhang, Q. Wang, Y. Xie, A partially penalised immersed finite element method for elliptic interface problems with non-homogeneous jump conditions, *East Asian Journal on Applied Mathematics* 8 (1).
- [19] P. Huang, Z. Li, Partially penalized ife methods and convergence analysis for elasticity interface problems, *Journal of Computational and Applied Mathematics* 382 (2020) 113059.
- [20] Q. Yang, Numerical analysis of partially penalized immersed finite element methods for hyperbolic interface problems, *Numerical Mathematics Theory Methods and Applications* 11 (002) (2018) 272–298.
- [21] W. Cao, X. Zhang, Z. Zhang, Q. Zou, Superconvergence of immersed finite element methods for interface problems, *Advances in Computational Mathematics* 43 (4) (2017) 795C821.
- [22] H. Guo, X. Yang, Gradient recovery for elliptic interface problem: II. immersed finite element methods, *Journal of Computational Physics* 338 (2017) 606–619.
- [23] H. Guo, X. Yang, Z. Zhang, Superconvergence of partially penalized immersed finite element methods, *IMA Journal of Numerical Analysis* 38 (4) (2017) 2123–2144.
- [24] C. He, X. Zhang, Residual-based a posteriori error estimation for immersed finite element methods, *Journal of Scientific Computing* 81 (3) (2019) 2051–2079.
- [25] O. C. Zienkiewicz, J. Z. Zhu, The superconvergent patch recovery and a posteriori error estimates. part 1: The recovery technique, *International Journal for Numerical Methods in Engineering* 33 (7) (1992) 1331–1364.
- [26] O. C. Zienkiewicz, J. Z. Zhu, The superconvergent patch recovery and a posteriori error estimates. part 2: Error estimates and adaptivity, *International Journal for Numerical Methods in Engineering* 33 (7) (1992) 1365–1382.
- [27] A. Naga, Z. Zhang, A posteriori error estimates based on the polynomial preserving recovery, *SIAM Journal on Numerical Analysis* 42 (4) (2004) 1780–1800.

- [28] Z. Zhang, A. Naga, The polynomial-preserving recovery for higher order finite element methods in 2d and 3d, *Discrete and Continuous Dynamical Systems - Series B (DCDS-B)* 5 (3) (2012) 769–798.
- [29] Z. Zhang, A. Naga, A new finite element gradient recovery method: superconvergence property, *SIAM Journal on Scientific Computing* 26 (4) (2005) 1192–1213.
- [30] Y. Huang, N. Yi, The superconvergent cluster recovery method, *Journal of Scientific Computing* 44 (3) (2010) 301–322.
- [31] Z. Cai, S. Zhang, Recovery-based error estimator for interface problems: conforming linear elements, *SIAM Journal on Numerical Analysis* 47 (3) (2009) 2132–2156.
- [32] M. Ainsworth, J. T. Oden, A posteriori error estimation in finite element analysis, *Comput.methods Appl.mech.engng* 142 (1-2) (1997) 1–88.
- [33] Y. Chen, Y. Huang, N. Yi, A scr-based error estimation and adaptive finite element method for the allen–cahn equation, *Computers and Mathematics with Applications* 78 (1) (2019) 204–223.
- [34] N. Yan, *Superconvergence analysis and a posteriori error estimation in finite element methods*, Science Press, 2008.
- [35] L. Mu, X. Zhang, An immersed weak galerkin method for elliptic interface problems, *Journal of Computational and Applied Mathematics* 362 (2019) 471–483.
- [36] T. Lin, Q. Yang, X. Zhang, A priori error estimates for some discontinuous galerkin immersed finite element methods, *Journal of Scientific Computing* 65 (3) (2015) 875–894.

School of Mathematical Sciences, South China Normal University, Guangzhou 510631, China  
*E-mail:* yanpingchen@scnu.edu.cn

School of Mathematics and Computational Science, Xiangtan University, Xiangtan, 411105, Hunan, Peoples Republic of China  
*E-mail:* 201921001130@smai1.xtu.edu.cn and huangyq@xtu.edu.cn